Bi-3 C^2 Polar Subdivision

Ashish Myles*
Jörg Peters†
University of Florida

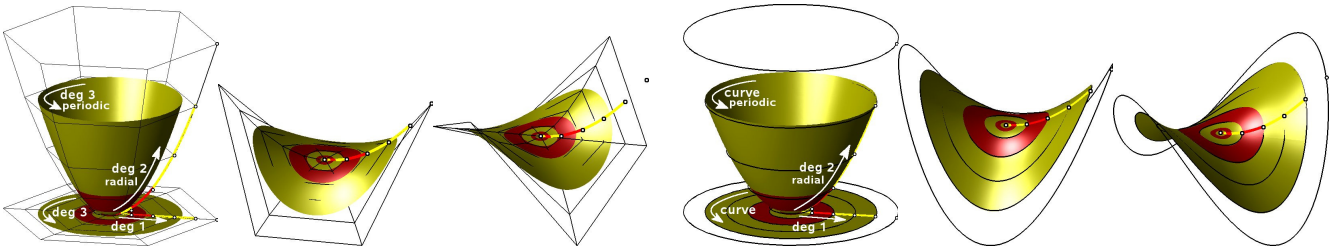

(a) e_3 (b) e_4 (c) e_5 (d) e_3: x^2+y^2 (e) e_4: x^2-y^2 (f) e_5: $2xy$

$n=6$: $e_3, e_4, e_5 \notin \text{span}\{e_1^2, e_1e_2, e_2^2\}$ $n \to \infty$: $e_3, e_4, e_5 \in \text{span}\{e_1^2, e_1e_2, e_2^2\} + \text{O}(\frac{1}{4^n})$

Figure 1: Making C^2 subdivision work with degree bi-3. *(left: a,b,c) Stationary degree bi-3 subdivision cannot be C^2 at a central point of fixed valence n since this requires that the subsubdominant* eigensplines e_3, e_4, e_5 *(*curved yellow and red paraboloid and saddles*) are quadratic in the characteristic subdominant eigensplines $\chi := (e_1, e_2)$ (*bottom planar disk*) and therefore that e_3, e_4 and e_5 are of degree 6 or higher in the periodic direction. (right: d,e,f) Increasing the valence $n \to \infty$ of a degree bi-3 subdivision algorithm in each step, however, allows enforcing the requirement* in the limit*, yielding a well-defined quadratic Taylor expansion. (left: a,b,c) The control nets (*black n=6*-valent polar configurations) represent the eigenvectors $\mathbf{v}_k$, $k=1,\ldots,5$. (right: d,e,f) As $n \to \infty$, the vectors $\mathbf{v}_k$ converge to periodic curves (*in black*). (a–f) The radial eigenvectors $\hat{\mathbf{v}}_k$ of the Fourier transform are control lines indicated by $\circ$. The corresponding radial eigensplines $\hat{e}_k$ are shown as* yellow and red curves.

Abstract

Popular subdivision algorithms like Catmull-Clark and Loop are C^2 almost everywhere, but suffer from shape artifacts and reduced smoothness exactly near the so-called "extraordinary vertices" that motivate their use. Subdivision theory explains that inherently, for standard stationary subdivision algorithms, curvature-continuity and the ability to model all quadratic shapes requires a degree of at least bi-6. The existence of a simple-to-implement C^2 subdivision algorithm generating surfaces of good shape and piecewise degree bi-3 in the polar setting is therefore a welcome surprise. This paper presents such an algorithm, the underlying insights, and a detailed analysis. In bi-3 C^2 polar subdivision the weights depend, as in standard schemes, only on the valence, but the valence at one central polar vertex increases to match Catmull-Clark-refinement.

CR Categories: I.3.5 [Computer Graphics]: Computational Geometry and Object Modeling—Curve, surface, solid, and object representations

Keywords: bicubic, bi-3, C^2, curvature continuous, polar, subdivision, surface, non-stationary

*e-mail: amyles@cise.ufl.edu
†e-mail: jorg@cise.ufl.edu

1 Introduction

A fundamental question when modeling geometry, dating back to the publication of the Catmull-Clark algorithm more than 30 years ago [Catmull and Clark 1978], is whether there exists a refinement algorithm for polyhedral meshes with a C^2 limit surface consisting of bi-degree 3 surface pieces only. Differently put, can we devise a surface representation that generalizes the widely used bi-3 C^2 splines to a non-tensor-product layout, where more or fewer than four polynomial patches meet at a given (extraordinary) point, without increasing the polynomial degree of the pieces above three? The landmark papers [Prautzsch and Reif 1999a; Prautzsch and Reif 1999b] proved that no such algorithm can exist in the Catmull-Clark setting, no matter how complex the stationary subdivision rules. Our paper proves that a bi-3 algorithm does exist for polar configurations and the algorithm has *simple rules*.

Bi-3 C^2 polar subdivision (C^2PS) needs not obey the degree-6 lower bound of stationary algorithms, since it doubles the valence at some isolated vertices, as shown in Figure 3(c,e). Unlike non-stationary schemes that change refinement masks while keeping valence constant, C^2PS rules rely neither on projection nor on auxiliary data that encodes state. The averaging weights depend only on the local connectivity. Therefore C^2PS is as easy to describe and implement as standard stationary algorithms (see rules (1)–(3) on page 3).

Polar configurations were introduced in [Karčiauskas et al. 2006] to cope with situations where vertices of high valence occur naturally such as illustrated in Figure 2. A *polar configuration* is a triangle fan surrounded by rings of quadrilaterals with 4-valent vertices (see Figure 3(c)). The fan center is the *polar vertex* and its limit point is called *pole*.

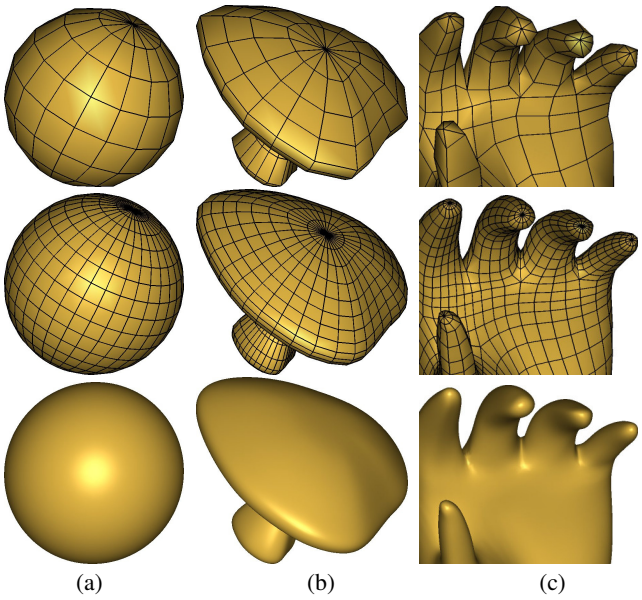

Figure 2: *(top)* **Polar configurations***: (a) globe, (b) mushroom, (c) finger tips; (middle) C^2PS subdivision; (bottom) C^2PS limit surface.*

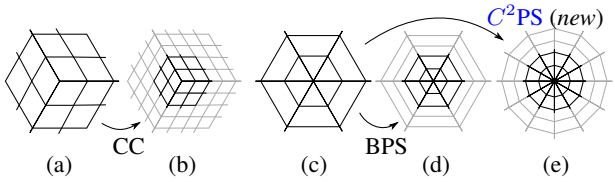

Figure 3: Connectivity. *Catmull-Clark refinement (a) to (b) retains the valence at the central point. (c) Polar configurations can be refined by (d) BPS, a stationary algorithm or, by (e) C^2PS, which doubles the polar valence.*

The *contribution* of this paper is then two-fold. For graphics modeling practice, we provide a mesh refinement algorithm for polar configurations that
— has simple rules;
— refines the mesh compatibly with Catmull-Clark subdivision;
— works well for high valences;
— constructs a surface that is C^2 also at the pole;
— is piecewise of degree bi-3; and
— allows modeling any quadratic shape at the pole.
For modeling theory,
— we propose algorithms that allow increasing valence; and
— provide the intuition and a rigorous analysis of one instance.
In fact, while the algorithm is easily described in a few lines on page 3, we devote a large part of the paper to convey the proof idea and to formally prove curvature continuity via an auxiliary subdivision scheme.

The paper is organized as follows. Section 3 defines C^2 polar subdivision. This section has all the information needed to implement the algorithm. Section 4 presents the underlying ideas and Section 5 a detailed analysis for the specialist. Section 6 reports tests and comparisons to other algorithms and Section 7 summarizes and lists limitations, extensions and future directions.

2 C^2 and polar subdivision literature

A number of algorithms have aimed at complementing and improving the smoothness and shape of Catmull-Clark subdivision at extraordinary points. [Prautzsch and Umlauf 1998] designed the first bicubic refinement algorithm that is C^2 in a weak sense – extraordinary points have forced zero curvature, resulting in flat-spots. TURBS [Reif 1998] offered C^k continuity of degree bi-$(2k+2)$; and [Ying and Zorin 2004] constructed C^∞ surfaces by blending polynomial patches with exponentials. [Zulti et al. 2006] adapted the three-direction box spline to be C^2 on an infinite mesh with a single extraordinary point. To directly improve the limit surface, [Levin 2006] perturbed Catmull-Clark surfaces using polynomial-square-root blending functions between local polynomial patches; [Zorin 2006] similarly perturbed Loop subdivision surfaces to be C^2 using a blending function that is itself a subdivision surface.

Other techniques improve smoothness by directly converting meshes to splines. Like TURBS, free-form splines [Prautzsch 1997] built C^k surfaces with degree bi-$(2k+2)$. [Peters 2002] used patches of degree $(3,5)$ that joined C^2. [Loop 2004; Loop and Schaefer 2008] built curvature continuous surfaces from quad meshes using bi-degree 7 patches, setting extra parameters by minimizing deviation from bi-degree 3 patches. [Karčiauskas and Peters 2007a; Karčiauskas and Peters 2008] introduced guided subdivision, capable of constructing C^k surfaces and in particular C^2 surfaces consisting of bi-6 spline rings that ever more closely follow a C^2 guide surface. In a report [Karčiauskas and Peters 2007b] show that an increasing number of guide-sampled bi-3 splines per ring can achieve the same C^2 continuity. Allowing such an increase is also the crucial ingredient in our approach, but arguably comes about more naturally in our algorithm.

Other mildly non-stationary algorithms adjust the uniform rules after each iteration step [Choi et al. 2006], or add tension parameters to Doo-Sabin subdivision [Zhang and Wang 2002] or to uniform bi-3 subdivision [Morin et al. 2001] (to produce trigonometric splines for surfaces of revolution). When the subdivision weights change with each step, the *proximity* technique of comparing to an auxiliary subdivision with stationary rules [Wallner and Dyn 2005] can often be used for analysis. We also compare to an auxiliary subdivision, but the non-stationarity in our case is not in the subdivision weights but in the connectivity.

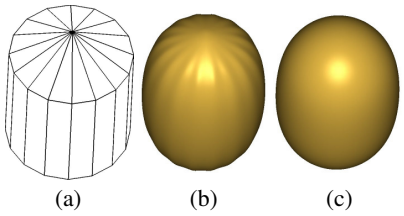

Figure 4: Avoiding ripples. *(a) Convex polar configuration, (b) corresponding Catmull-Clark subdivision surface, and (c) C^2PS surface.*

[Karčiauskas et al. 2006] observed that unintended ripples near vertices of high valence, such as in Figure 4(b), can be avoided by switching to algorithms acting on polar configurations. Their jet subdivision algorithm generates flexible C^2 surfaces of degree $(6,5)$. Bicubic polar subdivision (BPS) uses much simpler rules, made compatible with Catmull-Clark subdivision in [Karčiauskas and Peters 2007c; Myles et al. 2008], that yield C^1 bi-3 limit surfaces. Figure 5 contrasts the refinement strategies of BPS, Catmull-Clark, and C^2 polar subdivision. BPS refines in a radial direction only, before applying any refinement in the periodic direction.

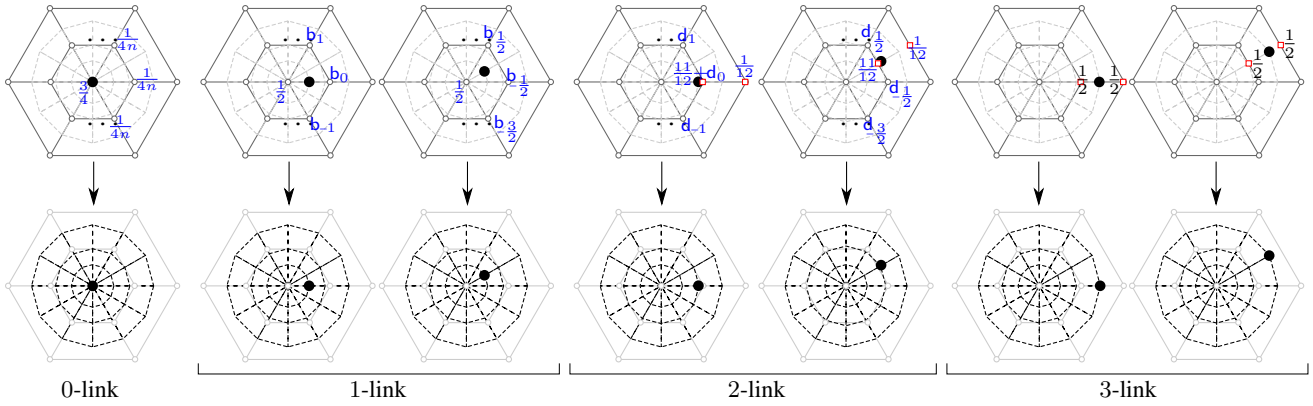

Figure 6: C^2 **polar subdivision rules.** *A polar configuration (*$\circ$, solid lines*) is refined using special rules* (1)–(3) *to compute the new 0-, 1-, and 2-link (*$\bullet$ *and* dashed lines*). For* $i > 2$*, the refined* i*-links are computed via uniform bi-3 subdivision. The weights* b_j *and* d_j *are defined by* (4)*. Vertices indicated by* $\square$ *are computed using uniform cubic subdivision* (5)*.*

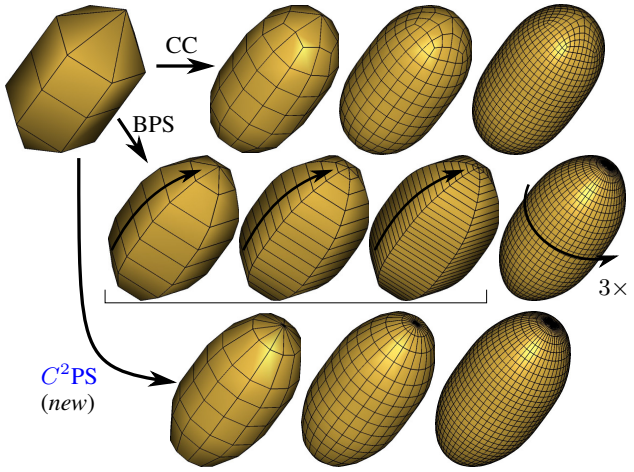

Figure 5: Comparison of refinement. *(top) Catmull-Clark subdivision (CC) splits every quad directly into four. (middle) Bicubic polar subdivision (BPS) refines in the radial direction repeatedly (here 3 times) and only then in the periodic direction* $3\times$ *to achieve the same granularity as Catmull-Clark. (bottom)* C^2*PS refines just like Catmull-Clark away from the polar vertex.*

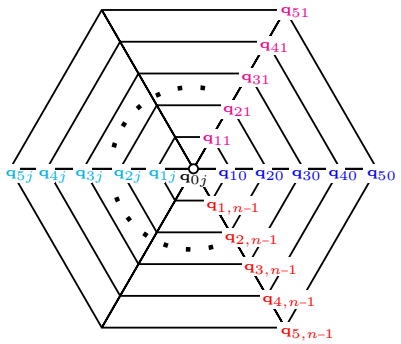

Figure 7: *A* **polar configuration** *with polar vertex* $\mathbf{q}_{00} = \mathbf{q}_{0j}$ *of valence* n*. Two rings suffice to get* C^2*PS started, five rings define a (double) surface ring (see Figure 9) used to formally analyze the algorithm in the limit.*

Compatibility with Catmull-Clark extraordinary vertices requires separate treatment of the two types of configurations. In contrast, C^2 polar subdivision refines compatibly with Catmull-Clark away from the polar configuration (Figure 5, *bottom*) simplifying a combined implementation as in Figure 2 (c).

3 C^2 polar subdivision

A *polar configuration* surrounds a central *polar vertex* by a fan of n triangles, and the fan by, possibly zero, rings of quadrilateral facets with 4-valent vertices (see Figure 7). We call the collection of vertices i (radial) edges away from the polar vertex its i*-link*. The polar vertex is its 0-link. Listing the polar vertex $\mathbf{q}_{0j} = \mathbf{q}_{00}$ repeatedly, the $6n$ vertices

$$\begin{aligned}\mathbf{q} := [&\mathbf{q}_{0,0}, \mathbf{q}_{1,0}, \ldots, \mathbf{q}_{5,0},\\ &\mathbf{q}_{0,1}, \mathbf{q}_{1,1}, \ldots, \mathbf{q}_{5,1}, \quad \ldots,\\ &\mathbf{q}_{0,n-1}, \mathbf{q}_{1,n-1}, \ldots, \mathbf{q}_{5,n-1}]^{\mathrm{T}},\end{aligned}$$

encode the polar configuration of Figure 7. We can traverse a polar configuration *radially*, visiting $[\mathbf{q}_{0,j}, \mathbf{q}_{1,j}, \ldots]$ as we move outwards, or *periodically*, circling the polar vertex on an i-link $[\mathbf{q}_{i,0}, \mathbf{q}_{i,1}, \ldots, \mathbf{q}_{i,n-1}]^{\mathrm{T}}$. The second index, j, is then interpreted modulo n.

Due to its small subdivision stencils, C^2 polar subdivision only requires the 0-, 1-, and 2-link, allowing the 2-link to contain an irregular vertex, such as another extraordinary vertex or a polar vertex. A polar vertex can be separated from irregular neighbors by *locally* inserting a new link between the 1-link and the polar vertex.

Rules of C^2PS (C^2 polar subdivision)
With $\mathbf{q}^0 := \mathbf{q}$, we obtain the $m+1$ times refined polar configuration $\mathbf{q}^{m+1}$ from $\mathbf{q}^m$ by the rules (see Figure 6)

$$\mathbf{q}_{00}^{m+1} := \frac{3}{4}\mathbf{q}_{00}^m + \frac{1}{4n_m}\sum_{h=0}^{n_m-1}\mathbf{q}_{1h}^m \tag{1}$$

$$\mathbf{q}_{1j}^{m+1} := \frac{1}{2}\mathbf{q}_{00}^m + \sum_{h=0}^{n_m-1}\mathsf{b}_{h-\frac{j}{2}}\mathbf{q}_{1h}^m \tag{2}$$

$$\mathbf{q}_{2j}^{m+1} := \frac{11}{12}\tilde{\mathbf{q}}_{1j}^m + \frac{1}{12}\tilde{\mathbf{q}}_{2j}^m + \sum_{h=0}^{n_m-1}\mathsf{d}_{h-\frac{j}{2}}\mathbf{q}_{1h}^m \tag{3}$$

where $c_\tau := \cos(2\pi\tau)$, $s_\tau := \sin(2\pi\tau)$, the valence of the polar

vertex at refinement m is $n_m := n2^m$,

$$\begin{aligned} \mathsf{b}_g &:= \frac{1}{n_m}\left(\frac{1}{2} + c_{g/n_m} + \frac{1}{2}c_{2g/n_m}\right), \\ \mathsf{d}_g &:= -\frac{1}{6n_m}c_{g/n_m}, \end{aligned} \tag{4}$$

and each i-link $\tilde{\mathbf{q}}_i^m$ of the intermediate polar configuration $\tilde{\mathbf{q}}^m$ is obtained from $\mathbf{q}_i^m$ by uniform degree-3 spline subdivision in the periodic direction:

$$\begin{aligned} \tilde{\mathbf{q}}_{i,2j}^m &:= \frac{1}{8}\mathbf{q}_{i,j-1}^m + \frac{6}{8}\mathbf{q}_{ij}^m + \frac{1}{8}\mathbf{q}_{i,j+1}^m \\ \tilde{\mathbf{q}}_{i,2j+1}^m &:= \frac{1}{2}\mathbf{q}_{ij}^m + \frac{1}{2}\mathbf{q}_{i,j+1}^m. \end{aligned} \tag{5}$$

For $i > 2$, the new i-links are determined by uniform bi-3 subdivision in both directions, the ordinary tensor-product spline subdivision rules used by Catmull-Clark subdivision.

For example, when $n_0 := 6$ and therefore $n_1 = 12$, the once-refined 1-link control points in Figure 6 are defined by

$$\mathbf{q}_{10}^1 := \frac{1}{2}\mathbf{q}_{00}^0 + \frac{1}{6}\sum_{h=0}^{5}\left(\frac{1}{2} + c_{h/6} + \frac{1}{2}c_{2h/6}\right)\mathbf{q}_{1h}^0$$

$$\mathbf{q}_{11}^1 := \frac{1}{2}\mathbf{q}_{00}^0 + \frac{1}{6}\sum_{h=0}^{5}\left(\frac{1}{2} + c_{(h-\frac{1}{2})/6} + \frac{1}{2}c_{2(h-\frac{1}{2})/6}\right)\mathbf{q}_{1h}^0.$$

4 The intuition underlying C^2PS

If we want to avoid shape defects, such as forced zero curvature, our subdivision must be able to reproduce quadratic functions at the pole; for example, $f(x, y) = x^2 + y^2$ yielding the paraboloid $(x, y, x^2 + y^2)$. While we can linearly trace out the radial direction from the polar vertex in the tangential xy-plane (see disk in Figure 1(a)), parametric C^2 continuity implies that the degree in the periodic direction can be no less than 3. But then, $z = x^2 + y^2$ has periodic degree at least 6 which exceeds the degree of the bi-3 patches in polar layout. This is the gist of the lower bound proofs of [Prautzsch and Reif 1999a; Prautzsch and Reif 1999b] with the planar disk playing the role of the characteristic map of the subdivision algorithm.

What saves the day is the freedom of our algorithm to increase the valence $n \to \infty$. Doubling the valence as we refine the i-links of the polar configuration results in a $O(\frac{1}{2^{3m}})$ error in the m^{th} subdivision step when approximating cos and sin. Because $\cos(2t)$ and $\sin(2t)$ are in the span of $\{\cos^2(t), \cos(t)\sin(t), \sin^2(t)\}$, exactly as the sufficient conditions for C^2 continuity require [Peters and Reif 2008, Thm 7.16], this allows subdivision in the limit as $n \to \infty$ to model the paraboloid as well as hyperbolic saddles (Figure 1(d–f)) at the pole.

While the above argument gives green light to the possibility of a C^2 subdivision algorithm of periodic degree 3, *proving* C^2 continuity of non-stationary schemes can be difficult. We devise an auxiliary *stationary* subdivision algorithm that can be analyzed by the established arsenal of techniques and then derive the explicit second-order Taylor-expansion of C^2PS at the pole by comparison to this auxiliary algorithm as $n \to \infty$.

5 Proof of curvature continuity

This formal analysis of curvature continuity is intended for the specialist. For a more gradual and detailed treatment, see [Myles 2008]. To prove that bi-3 C^2PS is C^2 at the pole, we
– define, in Section 5.2, the auxiliary stationary subdivision algorithm RTS to reproduce any quadratic in the radial direction;
– show, in Section 5.3, that the eigensplines of RTS approximate as $n \to \infty$ the quadratic (Taylor) basis

$$T_2 := \{1, x, y, x^2 + y^2, x^2 - y^2, 2xy\}.$$

– leverage this in Section 5.4 to show that the eigensplines of C^2PS reproduce T_2 at the pole; and
– exhibit T_2 at the pole explicitly, in Section 5.5.

5.1 Subdivision Basics

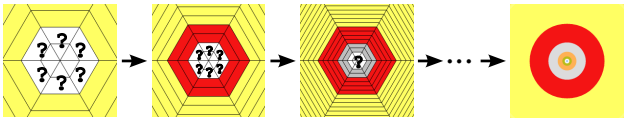

Figure 8: Nested bi-3 spline rings *converging to the pole (generated by BPS or RTS subdivision).*

As illustrated in Figure 8, the neighborhood of a subdivision pole consists of an infinite sequence of spline surface rings generated by the iterative refinement process. As we analyze this sequence to derive an explicit Taylor expansion at the pole, it suffices to consider one coordinate $\mathbf{q}_{ij} \in \mathbb{R}$ of the limit surface $\mathbf{x} =: \mathcal{L}(\mathbf{q})$. We will superscript $\mathbf{x}$ and the operator $\mathcal{L}$ by C^2PS or RTS, when needed. Below
$\mathbb{Z}_n$ denotes the integers $\mathbb{Z}$ modulo n;
$\mathcal{Z}_n$ the sequence $0, 1, \ldots, n-1$;
$\mathbb{R}_1$ the reals $\mathbb{R}$ modulo 1; and
for integers n, $\sum_h^n$ denotes $\sum_{h=0}^{n-1}$.
The *spline ring* corresponding to the 5-link $\mathbf{q}^m$ (see Figure 9) is the map

$$\begin{aligned} &G_m\mathbf{q}^m : [2\lambda^m, 4\lambda^m] \times \mathbb{R}_1 \to \mathbb{R}, \\ &(G_m\mathbf{q}^m)(r,\tau) := \sum_{i=1}^{5}\sum_{j}^{n} \mathbf{q}_{ij}^m \mathring{N}_i^{*(m)}(r)\mathring{N}_j^{\circ(n_m)}(\tau) \end{aligned} \tag{6}$$

with B-spline control points

$$\mathbf{q}_{ij}^m, i \in \{1,2,3,4,5\}, j \in \mathbb{Z}_n, n \geq 3, \tag{7}$$

where the radial and the periodic direction of the tensor-product are uniform degree 3 B-splines (see e.g. [Farin 1997; Prautzsch et al. 2002])

- (radial) $\mathring{N}_i^{*(m)}(r)$ with knots $\lambda^m[-1, 0, 1, 2, 3, 4, 5, 6, 7]$, where $\lambda := \frac{1}{2}$.
- (periodic) $\mathring{N}_j^{\circ(n)}(\tau)$ with periodic knots $\frac{1}{n}\mathcal{Z}_n$.

Since $\lambda = \frac{1}{2}$, the radial parameter of each spline ring halves after every subdivision. We note that the periodic direction is parameterized by $\mathbb{R}_1$ rather than $\mathbb{R}_{2\pi}$ and that $G_m\mathbf{q}^m$ is linear with respect to $\mathbf{q}^m$.

Each coordinate $\mathbf{x} : [0, 4] \times \mathbb{R}_1 \to \mathbb{R}$ of the *polar limit surface* (in $\mathbb{R}^3$) is defined piecewise in terms of surface rings

$$\mathbf{x}(r,\tau)\big|_{r\in[2\lambda^m, 4\lambda^m]} := (G_m\mathbf{q}^m)(r,\tau). \tag{8}$$

The unique limit $\mathbf{x}(0, \tau)$ is called *pole*.

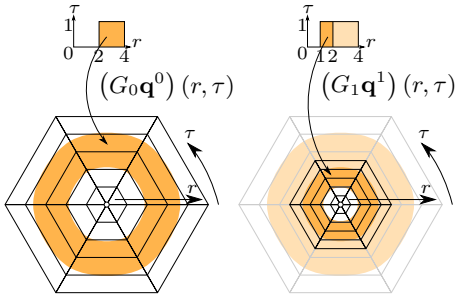

Figure 9: Each subdivision step generates a new surface ring. *The m-times subdivided polar configuration $\mathbf{q}^m$ defines a double bi-3 spline ring $(G_m\mathbf{q}^m)(r,\tau)$ (*orange*) via* (6)*. The radial parameter shrinks by half after each subdivision so that $r \in [2,4]$ for $G_0\mathbf{q}^0(r,\tau)$ and $r \in [1,2]$ for $(G_1\mathbf{q}^1)(r,\tau)$.*

5.2 RTS definition and analysis

Here we introduce RTS (radial Taylor subdivision), a stationary polar subdivision algorithm whose refinement action is illustrated in Figure 3(c,d), the same as BPS, shown in Figure 5, *middle*. We note that in Sections 5.2 and 5.3, $\mathbf{q}^m$ denotes control points generated by RTS.

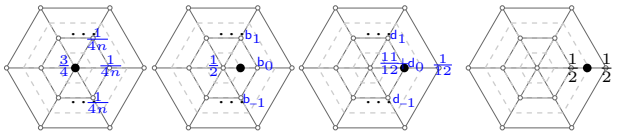

Figure 10: Radial Taylor subdivision *(RTS) subdivides strictly in the radial direction to compute vertices (•) on the refined mesh (*light gray, dashed*) as a linear combination of the old mesh (*dark gray*, vertices as ∘). As in C^2PS, uniform degree-3 rules are applied beyond the refined 2-link.*

Definition 1 (Radial Taylor subdivision)**.** Radial Taylor subdivision*, or* RTS*, refines an n-sided polar configuration $\mathbf{q}^m$ to the n-sided polar configuration $\mathbf{q}^{m+1}$ defined by (see Figure 10)*

$$\mathbf{q}_{00}^{m+1} := \frac{3}{4}\mathbf{q}_{00}^m + \frac{1}{4n}\sum_h^n \mathbf{q}_{1h}^m \tag{9}$$

$$\mathbf{q}_{1j}^{m+1} := \frac{1}{2}\mathbf{q}_{00}^m + \sum_h^n \mathsf{b}_{h-j}\mathbf{q}_{1h}^m \tag{10}$$

$$\mathbf{q}_{2j}^{m+1} := \frac{11}{12}\mathbf{q}_{1j}^m + \frac{1}{12}\mathbf{q}_{2j}^m + \sum_h^n \mathsf{d}_{h-j}\mathbf{q}_{1h}^m \tag{11}$$

$$\mathbf{q}_{3j}^{m+1} := \frac{1}{2}\mathbf{q}_{1j}^m + \frac{1}{2}\mathbf{q}_{2j}^m \qquad \mathbf{q}_{4j}^{m+1} := \frac{1}{8}\mathbf{q}_{1j}^m + \frac{6}{8}\mathbf{q}_{2j}^m + \frac{1}{8}\mathbf{q}_{3j}^m$$

$$\mathbf{q}_{5j}^{m+1} := \frac{1}{2}\mathbf{q}_{2j}^m + \frac{1}{2}\mathbf{q}_{3j}^m \tag{12}$$

with b_j and d_j defined in (4)*. The new* 3*-,* 4*-, and* 5*-links are determined by uniform degree 3 refinement in the radial direction. As in* (8)*, the limit surface $\mathbf{x}^{\mathrm{RTS}}$ consists of nested spline rings $G_m\mathbf{q}^m$.*

The equations defining RTS are intentionally very similar to those of C^2PS ((1)–(3)) since RTS serves as an auxiliary subdivision whose surface rings will be compared to those of C^2PS.

Distributing the contribution of the polar vertex $\mathbf{q}_{00}^m$ among its n copies $\mathbf{q}_{0j}^m$, $j \in \mathbb{Z}_n$, one can write RTS compactly as a multiplication by a $6n \times 6n$ block-circulant subdivision matrix A:

Table 1: *The* **dominant spectrum of RTS**. *The left ($\hat{\mathbf{w}}_k$) and right ($\hat{\mathbf{v}}_k$) eigenvectors $\hat{A}$ to the eigenvalue λ_k of the Fourier block α_k are normalized so that the related vectors $\mathbf{w}_k$ and $\mathbf{v}_k$ satisfy $\mathbf{w}_{k_1}^{\mathrm{T}}\mathbf{v}_{k_2} = \delta_{k_1 k_2}$.*

k	α_k	λ_k	$\hat{\mathbf{w}}_k^{\mathrm{T}}$ (left eigenv.)	$\hat{\mathbf{v}}_k^{\mathrm{T}}$ (right eigenvector)
0	0	1	$\frac{1}{3}[2,1,0,0,0,0]$	$[1,1,1,1,1,1]$
1	1	1/2	$[0,2,0,0,0,0]$	$[0,1,2,3,4,5]$
2	n–1	1/2	$[0,2,0,0,0,0]$	$[0,1,2,3,4,5]$
3	0	1/4	$[-1,1,0,0,0,0]$	$\frac{1}{3}[-1,2,11,26,47,74]$
4	2	1/4	$[0,3,0,0,0,0]$	$\frac{1}{3}[0,2,11,26,47,74]$
5	n–2	1/4	$[0,3,0,0,0,0]$	$\frac{1}{3}[0,2,11,26,47,74]$

$$\mathbf{q}^{m+1} = A\mathbf{q}^m, \text{where} \tag{13}$$

$$A := \begin{bmatrix} A_0 & A_1 & \cdots & A_{n-1} \\ A_{n-1} & A_0 & \cdots & A_{n-2} \\ \vdots & & \ddots & \vdots \\ A_1 & \cdots & A_{n-1} & A_0 \end{bmatrix},$$

$$A_0 := \begin{bmatrix} \frac{3}{4n} & \frac{1}{4n} & 0 & 0 & 0 & 0 \\ \frac{1}{2n} & \mathsf{b}_0 & 0 & 0 & 0 & 0 \\ 0 & \frac{11}{12}+\mathsf{d}_0 & \frac{1}{12} & 0 & 0 & 0 \\ 0 & \frac{1}{2} & \frac{1}{2} & 0 & 0 & 0 \\ 0 & \frac{1}{8} & \frac{3}{4} & \frac{1}{8} & 0 & 0 \\ 0 & 0 & \frac{1}{2} & \frac{1}{2} & 0 & 0 \end{bmatrix}, \quad A_{\substack{j \\ (j\neq 0)}} := \begin{bmatrix} \frac{3}{4n} & \frac{1}{4n} & 0 & 0 & 0 & 0 \\ \frac{1}{2n} & \mathsf{b}_j & 0 & 0 & 0 & 0 \\ 0 & \mathsf{d}_j & 0 & 0 & 0 & 0 \\ 0 & 0 & 0 & 0 & 0 & 0 \\ 0 & 0 & 0 & 0 & 0 & 0 \\ 0 & 0 & 0 & 0 & 0 & 0 \end{bmatrix}.$$

Only the first 3×3 block of the subdivision matrix has non-standard weights. The remainder applies uniform degree-3 spline subdivision in the radial direction. Since we are interested in the behavior of the algorithm for high polar valences, we stipulate that $n \geq 5$. This guarantees at least five non-overlapping blocks A_j, $j \in \{0,1,2,n-2,n-1\}$, along the diagonal. To facilitate spectral analysis, the block circulant A is block diagonalized via the discrete Fourier transform to

$$\hat{A} := \begin{bmatrix} \hat{A}_0 & \mathbf{0} & \cdots & \mathbf{0} \\ \mathbf{0} & \hat{A}_1 & & \mathbf{0} \\ \vdots & & \ddots & \vdots \\ \mathbf{0} & \cdots & \mathbf{0} & \hat{A}_{n-1} \end{bmatrix}, \quad \hat{A}_\alpha := \sum_j^n \omega^{-j\alpha} A_j,$$

with $\omega := \exp\left(\frac{2\pi\sqrt{-1}}{n}\right)$ and $\alpha \in \mathbb{Z}_n$. The Fourier blocks simplify to

$$\hat{A}_0 = \begin{bmatrix} \frac{3}{4} & \frac{1}{4} & 0 & 0 & 0 & 0 \\ \frac{1}{2} & \frac{1}{2} & 0 & 0 & 0 & 0 \\ 0 & \frac{11}{12} & \frac{1}{12} & 0 & 0 & 0 \\ 0 & \frac{1}{2} & \frac{1}{2} & 0 & 0 & 0 \\ 0 & \frac{1}{8} & \frac{3}{4} & \frac{1}{8} & 0 & 0 \\ 0 & 0 & \frac{1}{2} & \frac{1}{2} & 0 & 0 \end{bmatrix}, \quad \underset{(\alpha\neq 0)}{\hat{A}_\alpha} = \hat{A}_{n-\alpha} = \begin{bmatrix} 0 & 0 & 0 & 0 & 0 & 0 \\ 0 & \hat{\mathsf{b}}_\alpha & 0 & 0 & 0 & 0 \\ 0 & \frac{11}{12}+\hat{\mathsf{d}}_\alpha & \frac{1}{12} & 0 & 0 & 0 \\ 0 & \frac{1}{2} & \frac{1}{2} & 0 & 0 & 0 \\ 0 & \frac{1}{8} & \frac{3}{4} & \frac{1}{8} & 0 & 0 \\ 0 & 0 & \frac{1}{2} & \frac{1}{2} & 0 & 0 \end{bmatrix},$$

$$\hat{\mathsf{b}}_\alpha := \sum_j^n \omega^{-j\alpha}\mathsf{b}_j = \begin{cases} \frac{1}{2} & \text{if } \alpha \in \{0,1,n-1\} \\ \frac{1}{4} & \text{if } \alpha \in \{2,n-2\} \\ 0 & \text{otherwise,} \end{cases}$$

$$\hat{\mathsf{d}}_\alpha := \sum_j^n \omega^{-j\alpha}\mathsf{d}_j = \begin{cases} -\frac{1}{12} & \text{if } \alpha \in \{1,n-1\} \\ 0 & \text{otherwise.} \end{cases}$$

Table 1 enumerates the absolute largest six eigenvalues of $\hat{A}$,

$$(\lambda_0,\lambda_1,\ldots,\lambda_5) = (1,\lambda,\lambda,\mu,\mu,\mu), \quad \lambda := \frac{1}{2}, \mu := \lambda^2,$$

with $\mu > |\lambda_k|$ for $k > 5$. The Fourier block $\hat{A}_0$ contributes λ_0 and λ_3, while $\hat{A}_1 = \hat{A}_{n-1}$ and $\hat{A}_2 = \hat{A}_{n-2}$ contribute $\lambda_1 = \lambda_2$ and $\lambda_4 = \lambda_5$, respectively. The sufficient conditions for C^2 continuity [Peters and Reif 2008, Section 7.1] require examining the eigenvectors and to show that they reproduce the Taylor expansion.

For $\alpha_k \in \mathbb{Z}_n$ and the eigenvalue λ_k contributed by $\hat{A}_{\alpha_k}$, let $\hat{\mathbf{v}}_k \in \mathbb{R}^6$ and $\hat{\mathbf{w}}_k \in \mathbb{R}^6$ denote, respectively, its right and left eigenvectors. The corresponding eigenvector $\mathbf{v}_k \in \mathbb{R}^{6n}$ of A is a polar configuration and may be computed from $\hat{\mathbf{v}}_k$ via the inverse Fourier transform as

$$(\mathbf{v}_k)_{ij} := (\hat{\mathbf{v}}_k)_i \ \mathrm{op}_k\left(\frac{j}{n}\right), \tag{14}$$

$$\mathrm{op}_k(\xi) := \begin{cases} c_{\alpha_k \xi} & \text{if } \alpha_k \le \frac{n}{2} \\ -s_{\alpha_k \xi} & \text{otherwise,} \end{cases}$$

i.e. $(\mathrm{op}_0(\xi), \mathrm{op}_1(\xi), \ldots, \mathrm{op}_5(\xi)) = (1, c_\xi, s_\xi, 1, c_{2\xi}, s_{2\xi})$. With $\hat{\mathbf{v}}_1 = \hat{\mathbf{v}}_2 = [0, 1, 2, 3, 4, 5]$ from $\hat{A}_{\alpha_1} = \hat{A}_{\alpha_2}$,

$$(\mathbf{v}_1)_{ij} := (\hat{\mathbf{v}}_1)_i \ c_{j/n} \quad \text{and} \quad (\mathbf{v}_2)_{ij} := (\hat{\mathbf{v}}_1)_i \ s_{j/n}$$

are the x- and y-coordinates of the control net defining the *characteristic spline* χ [Peters and Reif 2008, Section 5.2]. The *eigenspline* $e_k := \mathcal{L}(\mathbf{v}_k)$ denotes the limit function of $\mathbf{v}_k$, and $\chi := (e_1, e_2)$ the characteristic spline. Figure 9 (and the saucer-like disks in Figure 1 a,b,c) illustrate this control net and spline. Injectivity and regularity of χ are easy to verify, guaranteeing a C^1 surface for generic input data. Together with the required spectral contribution described in the previous paragraph, this implies limit surfaces of bounded curvature.

For stationary schemes, the leap from bounded curvature to C^2 requires, additionally, that e_3, e_4, and e_5 contribute no more than the homogeneous quadratics of the Taylor basis in characteristic parameterization: $\mathrm{span}\{e_3, e_4, e_5\} \subset \mathrm{span}\{e_1^2, e_2^2, e_1 e_2\}$ [Peters and Reif 2008, Section 7.3]. Since functions quadratic in χ have periodic degree 6, a stationary bi-3 algorithm can only satisfy the constraint when $e_3 = e_4 = e_5 = 0$.

5.3 Taylor basis reproduction by RTS

By (14), we can split the eigensplines e_k into radial and periodic factors. We denote the radial eigenspline $\hat{e}_k$ as the limit curve of $\hat{\mathbf{v}}_k$, defined piecewise as

$$\hat{e}_k(r)\big|_{r \in [2\lambda^m, 4\lambda^m]} := \left(\hat{G}_m\left(\hat{A}^m_{\alpha_k}\hat{\mathbf{v}}_k\right)\right)(r) \tag{15}$$

where the operator $\hat{G}_m$ is a simpler version of the operator G_m that works strictly in the radial direction. For some vector $\mathbf{u} \in \mathbb{R}^6$, $\hat{G}_m\mathbf{u} : [2\lambda^m, 4\lambda^m] \to \mathbb{R}$ is the degree 3 spline defined by the B-spline control points $\mathbf{u}_i$, with $i \in \{1, 2, 3, 4, 5\}$:

$$\left(\hat{G}_m\mathbf{u}\right)(r) := \sum_{i=1}^{5} \mathbf{u}_i \mathring{N}_i^{(m)}(r). \tag{16}$$

Like G_m, the operator $\hat{G}_m$ is linear with respect to its parameter $\mathbf{u}$.

We use the operator

$$\mathrm{B}^n : u \mapsto \sum_j^n u\left(\frac{j}{n}\right) \mathring{N}_j^{(n)} \tag{17}$$

that uniformly samples any function $u : \mathbb{R} \to \mathbb{R}$ and interprets the samples as the control points of a uniform periodic spline.

Lemma 1. *The eigenspline e_k factors according to*

$$e_k(r, \tau) = \hat{e}_k(r) \ \mathrm{B}^n\mathrm{op}_k(\tau) \tag{18}$$

Proof. For $r \in [2\lambda^m, 4\lambda^m]$, $\quad e_k(r,\tau) \overset{(8)}{:=} \left(G_m\mathbf{v}_k^m\right)(r,\tau)$

$$\overset{\substack{(6)\\(13)}}{=} \sum_{i=1}^{5}\sum_{j}^{n} \big(\underbrace{A^m\mathbf{v}_k}_{\lambda_k^m\mathbf{v}_k}\big)_{ij} \ \mathring{N}_i^{*(m)}(r)\mathring{N}_j^{\circ(n)}(\tau)$$

$$\overset{(14)}{=} \sum_{i=1}^{5}\sum_{j}^{n} \big(\underbrace{\lambda_k^m\hat{\mathbf{v}}_k}_{\hat{A}^m_{\alpha_k}(\hat{\mathbf{v}}_k)}\big)_i \ \mathrm{op}_k\left(\frac{j}{n}\right) \ \mathring{N}_i^{*(m)}(r)\mathring{N}_j^{\circ(n)}(\tau)$$

$$= \left(\sum_{i=1}^{5}\left(\hat{A}^m_{\alpha_k}(\hat{\mathbf{v}}_k)\right)_i \mathring{N}_i^{*(m)}(r)\right)\left(\sum_j^n \mathrm{op}_k\left(\frac{j}{n}\right)\mathring{N}_j^{\circ(n)}(\tau)\right)$$

$$\overset{(16)}{=} \left(\hat{G}_m\left(\hat{A}^m_{\alpha_k}(\hat{\mathbf{v}}_k)\right)\right)(r) \ \ \mathrm{B}^n\mathrm{op}_k(\tau)$$

$$\overset{(15)}{=} \hat{e}_k(r) \ \ \mathrm{B}^n\mathrm{op}_k(\tau)$$

□

The factorization (18) makes it evident that e_k, like op_k, is periodic in τ with a period of $\frac{1}{\alpha_k}$, which is a direct consequence of $\mathbf{v}_k$ having frequency mode α_k. And, since operators G_m and $\hat{G}_m$ are linear, eigensplines and radial eigensplines inherit the scaling property

$$e_k(\lambda r, \tau) = \lambda_k e_k(r, \tau) \quad \text{and} \quad \hat{e}_k(\lambda r) = \lambda_k \hat{e}_k(r) \tag{19}$$

that allows characterizing the first six radial eigensplines in the following key lemma.

Lemma 2 (Radial Taylor basis reproduction)**.** *For $r \in [0, 4]$,*

$$\hat{e}_0(r) = 1 \tag{20}$$

$$\hat{e}_1(r) = \hat{e}_2(r) = r \tag{21}$$

$$\hat{e}_3(r) = \hat{e}_4(r) = \hat{e}_5(r) = r^2 \tag{22}$$

$$\hat{e}_k(r) = \mathrm{o}(r^2) \qquad \text{as } r \to 0 \text{ for } k > 5 \tag{23}$$

which imply, by Lemma 1, that

$$\begin{array}{lll} e_0(r,\tau) = 1, & e_1(r,\tau) = r \ \mathrm{B}^n c_\tau, & e_2(r,\tau) = r \ \mathrm{B}^n s_\tau, \\ e_3(r,\tau) = r^2, & e_4(r,\tau) = r^2 \ \mathrm{B}^n c_{2\tau}, & e_5(r,\tau) = r^2 \ \mathrm{B}^n s_{2\tau} \\ e_k(r,\tau) = \mathrm{o}(r^2) & \text{as } r \to 0 \text{ for } k > 5, & \end{array}$$

where $\mathrm{B}^n c_{\alpha\tau}$ means $\left(\mathrm{B}^n(\gamma \mapsto c_{\alpha\gamma})\right)(\tau)$, i.e. the operator B^n is applied to the function $\gamma \mapsto c_{\alpha\gamma} := \cos(2\pi\alpha\gamma)$, and the resulting spline is evaluated at τ. Analogously, $\left(\mathrm{B}^n(\gamma \mapsto s_{\alpha\gamma})\right)(\tau)$ is shortened to $\mathrm{B}^n s_{\alpha\tau}$.

Proof. The subdivision matrix A of RTS was specifically constructed to enable this lemma. The right eigenvectors of A listed in Table 1, interpreted as degree 3 B-spline control points, reproduce constant (for $k = 0$), linear (for $k = 1, 2$), and quadratic (for $k = 3, 4, 5$) polynomials respectively for $r \in [2, 4]$. The scaling relation (19) then implies (20), (21), and (22), i.e. reproduction of the polynomial on $[0, 4]$. When $k > 5$, using $\bar{r} := \frac{r}{\lambda^m}$ and restricting $r \in [2\lambda^m, 4\lambda^m]$ (i.e. bounding $\bar{r} \in [2, 4]$ away from 0 and ∞) gives (23):

$$\begin{aligned} \hat{e}_k(r) \quad &= \hat{e}_k(\lambda^m\bar{r}) \overset{(19)}{=} \lambda_k^m \hat{e}_k(\bar{r}) = \mathrm{o}(\mu^m)\hat{e}_k(\bar{r}) \\ &= \mathrm{o}(\mu^m) = \mathrm{o}(\mu^m\bar{r}^2) = \mathrm{o}\left((\lambda^m\bar{r})^2\right) = \mathrm{o}(r^2). \end{aligned}$$

□

To reproduce the bivariate Taylor basis in polar parameterization, also the periodic direction must have the correct form. The following lemma states that this is achieved when $n \to \infty$.

Lemma 3. *Let $\mathbf{v}_k^{[n]}$ be the eigenvector corresponding to a polar vertex of valence n, and $e_k^{[n]}$ its limit function. Then*

$$e_k^{[n]}(r,\tau) - \hat{e}_k(r)\,\mathrm{op}_k(\tau) = \mathrm{O}\left(\frac{1}{n^2}\right), \tag{24}$$

implying that $e_k^{[\infty]}(r,\tau) := \lim_{n\to\infty} e_k^{[n]}(r,\tau) = \hat{e}_k(r)\,\mathrm{op}_k(\tau)$.

Proof. By Lemma 1, noting that $\hat{e}_k(r)$ is independent of the valence,

$$e_k^{[n]}(r,\tau) - \hat{e}_k(r)\,\mathrm{op}_k(\tau) = \hat{e}_k(r)\left(\mathrm{B}^n\mathrm{op}_k(\tau) - \mathrm{op}_k(\tau)\right).$$

Since the linear interpolant of $\mathrm{op}_k(\tau)$ is the control polygon of $\mathrm{B}^n\mathrm{op}_k(\tau)$, we can prove the lemma via the triangle inequality by bounding the distance between

1. $\mathrm{B}^n\mathrm{op}_k(\tau)$ and its control polygon, and
2. $\mathrm{op}_k(\tau)$ and its linear interpolant.

1. For uniform degree 3 splines with control points $[\mathbf{q}_{ij}]_{j=0}^{n-1}$, the distance between the control polygon and the spline is proportional to the second differences of the control points $\mathbf{q}_{ij} = \mathrm{op}_k\left(\frac{j}{n}\right)$ [Lutterkort and Peters 2001]:

$$\begin{aligned}
&\frac{1}{6}\max_j\{|\mathbf{q}_{i,j-1} - 2\mathbf{q}_{ij} + \mathbf{q}_{i,j+1}|\}\\
=&\frac{1}{3}\max_j\left\{\left|\mathrm{op}_k\left(\frac{j}{n}\right)\right|\left|\left(c_{\alpha_k/n} - 1\right)\right|\right\} \qquad |\,\mathrm{op}_k(\tau)| \le 1\\
\le&\frac{1}{3}\max_j\left\{1 - c_{\alpha_k/n}\right\} \overset{\text{Taylor expan.}}{=} \mathrm{O}\left(\frac{\alpha_k^2}{n^2}\right) = \mathrm{O}\left(\frac{1}{n^2}\right).
\end{aligned}$$

2. For a C^2 function $f : [a,b] \in \mathbb{R} \to \mathbb{R}$, a Taylor expansion at a shows that a piecewise linear interpolant with distance $\frac{1}{n}$ between breakpoints approximates f with a deviation of $\mathrm{O}\left(\frac{1}{n^2}\max_{[a,b]}\{f''\}\right)$. Consequently, the piecewise linear interpolant to $\mathrm{op}_k(\tau)$ converges $\mathrm{O}\left(\frac{\alpha_k^2}{n^2}\right) = \mathrm{O}\left(\frac{1}{n^2}\right)$. □

Lemma 3 implies reproduction of the polar Taylor expansion up to degree 2 in the limit:

$$\left(e_0^{[\infty]}, e_1^{[\infty]}, \ldots, e_5^{[\infty]}\right)(r,\tau) = (1, rc_\tau, rs_\tau, r^2, r^2c_{2\tau}, r^2s_{2\tau}).$$

Below, we show C^2PS to behave similarly at the pole.

5.4 Taylor basis reproduction by C^2PS

To compare RTS and C^2PS, we eigen-expand

$$\mathbf{q} = \sum_k^{6n} \mathbf{p}_k\ \mathbf{v}_k \quad \Rightarrow \quad \mathbf{x}^{\mathrm{RTS}}(r,\tau) = \sum_k^{6n} \mathbf{p}_k\ e_k(r,\tau). \tag{25}$$

If $\mathbf{w}_k$ is the left eigenvector of A satisfying $\mathbf{w}_{k_1}^{\mathrm{T}}\mathbf{v}_{k_2} = \delta_{k_1k_2}$ the *eigencoefficients* are defined by $\mathbf{p}_k := \mathbf{w}_k^{\mathrm{T}}\mathbf{q}$ [Peters and Reif 2008, Section 4.6]. This eigenvector $\mathbf{w}_k$ is computed via inverse Fourier transform from the left eigenvector $\hat{\mathbf{w}}_k$ of A_{α_k}, yielding

$$\mathbf{p}_k := \mathbf{w}_k^{\mathrm{T}}\mathbf{q} = \sum_i^6\sum_j^n \underbrace{\frac{1}{n}\ (\hat{\mathbf{w}}_k)_i\ \ \mathrm{op}_k\left(\frac{j}{n}\right)}_{(\mathbf{w}_k)_{ij}}\ \mathbf{q}_{ij}. \tag{26}$$

Specifically, for $k \in \mathbb{Z}_6$ (see $\hat{\mathbf{w}}_k^{\mathrm{T}}$ in Table 1),

$$\begin{aligned}
&\beta := \tfrac{2}{3}\\
\mathbf{p}_0 &:= \beta\mathbf{q}_{00} + \tfrac{1-\beta}{n}\textstyle\sum_j^n \mathbf{q}_{1j}, \qquad \mathbf{p}_3 := \beta\left(-\mathbf{q}_{00} + \frac{1}{n}\sum_j^n \mathbf{q}_{1j}\right),\\
\mathbf{p}_1 &:= \tfrac{2}{n}\textstyle\sum_j^n c_{j/n}\mathbf{q}_{1j}, \qquad \mathbf{p}_4 := \frac{1}{n}\sum_j^n c_{2j/n}\mathbf{q}_{1j},\\
\mathbf{p}_2 &:= \tfrac{2}{n}\textstyle\sum_j^n s_{j/n}\mathbf{q}_{1j}, \qquad \mathbf{p}_5 := \frac{1}{n}\sum_j^n s_{2j/n}\mathbf{q}_{1j}
\end{aligned} \tag{27}$$

and

$$\mathbf{p}_k^m := \mathbf{w}_k^{\mathrm{T}}\mathbf{q}^m = \mathbf{w}_k^{\mathrm{T}}(A^m\mathbf{q}) = (\mathbf{w}_k^{\mathrm{T}}A^m)\mathbf{q} = \lambda_k^m\mathbf{w}_k^{\mathrm{T}}\mathbf{q} = \lambda_k^m\mathbf{p}_k.$$

Consequently,

$$\begin{aligned}
A^m\mathbf{q} &= \sum_k^{6n} \mathbf{p}_k^m\ \ \mathbf{v}_k\\
(A^m\mathbf{q})_{ij} &= \mathbf{p}_0 + \lambda^m(\hat{\mathbf{v}}_1)_i\left(\mathbf{p}_1c_{j/n} + \mathbf{p}_2s_{j/n}\right)\\
&\quad + \mu^m\big((\hat{\mathbf{v}}_3)_i\mathbf{p}_3 + (\hat{\mathbf{v}}_4)_i\big(\mathbf{p}_4c_{2j/n} + \mathbf{p}_5s_{2j/n}\big)\big) + \mathrm{o}(\mu^m)
\end{aligned} \tag{28}$$

for $i \in \mathbb{Z}_6$ and $\tau \in \frac{1}{n}\mathbb{Z}_n$. Substituting $\mathbf{p}_{k\in\mathbb{Z}_6}$ in (28) shows that the $\mathrm{o}(\mu^m)$ term is *identically 0* for each $i \in \mathbb{Z}_6$. Hence, this formulation can serve as an alternative definition of RTS.

To compare with C^2PS, we define its refinement operator.

Definition 2 (C^2 polar subdivision operator)**.** *The operator $\mathcal{T}$ applies the rules* (1)–(3) *and the degree 3 subdivision rules*

$$\begin{aligned}
\mathbf{q}_{3j}^{m+1} &:= \frac{1}{2}\tilde{\mathbf{q}}_{1j}^m + \frac{1}{2}\tilde{\mathbf{q}}_{2j}^m \qquad \mathbf{q}_{5j}^{m+1} := \frac{1}{2}\tilde{\mathbf{q}}_{2j}^m + \frac{1}{2}\tilde{\mathbf{q}}_{3j}^m\\
\mathbf{q}_{4j}^{m+1} &:= \frac{1}{8}\tilde{\mathbf{q}}_{1j}^m + \frac{6}{8}\tilde{\mathbf{q}}_{2j}^m + \frac{1}{8}\tilde{\mathbf{q}}_{3j}^m.
\end{aligned} \tag{29}$$

to refine an n_m-sided polar configuration $\mathbf{q}^m$ to a $2n_m$-sided polar configuration $\mathbf{q}^{m+1} := \mathcal{T}\mathbf{q}^m$. The corresponding limit surface $\mathbf{x}^{C^2PS}$ is piecewise defined by (8)*.*

The Appendix proves that

$$\begin{aligned}
\mathcal{T}^m\mathbf{q} &= \sum_k^{6n} \mathbf{p}_k^m\ \ \mathbf{v}_k\\
(\mathcal{T}^m\mathbf{q})_{ij} &= \mathbf{p}_0 + \lambda^m(\hat{\mathbf{v}}_1)_i\left(\mathbf{p}_1c_{j/n} + \mathbf{p}_2s_{j/n}\right)\\
&\quad + \mu^m\big((\hat{\mathbf{v}}_3)_i\mathbf{p}_3 + (\hat{\mathbf{v}}_4)_i\big(\mathbf{p}_4c_{2j/n} + \mathbf{p}_5s_{2j/n}\big)\big) + \mathrm{O}\left(\frac{1}{8^m}\right)
\end{aligned} \tag{30}$$

and the $\mathrm{O}\left(\frac{1}{8^m}\right)$ term is 0 for $i \in \{0,1\}$. The expansion (28) and (30) invite comparison of $A^m\mathbf{q}$ (for RTS) with $\mathcal{T}^m\mathbf{q}$ (for C^2PS). We note that A has $6n$ columns.

Lemma 4. *Let $\mathbf{v}_k$, $k \in \mathbb{Z}_{6n_0}$, be the k^{th} eigenvector of RTS with polar valence n_0. Then the* eigenspline $f_k := \mathcal{L}^{C^2\mathrm{PS}}(\mathbf{v}_k)$ of C^2PS *converges to $e_k^{[\infty]}$ at the pole:*

$$\left|f_k(r,\tau) - e_k^{[\infty]}(r,\tau)\right|_{r\in[2\lambda^m, 4\lambda^m]} = \mathrm{o}\left(\mu^m\right) \tag{31}$$

For $k = 0$, the right-hand-side is identically 0.

Proof. For $k = 0$, $f_0(r,\tau) = 1 = e_0^{[\infty]}(r,\tau)$ since both RTS and C^2PS are affine invariant. For $k > 0$, $|\lambda_k| \le \lambda$ and $r \in$

$[2\lambda^m, 4\lambda^m]$, $\bar{r} := \frac{r}{\lambda^m}$,

$$
\begin{aligned}
E := \left| f_k(r,\tau) - e_k^{[\infty]}(r,\tau) \right| &= \left| f_k(\lambda^m \bar{r},\tau) - e_k^{[\infty]}(\lambda^m \bar{r},\tau) \right| \\
&\le \left| f_k(\lambda^m \bar{r},\tau) - e_k^{[n_m]}(\lambda^m \bar{r},\tau) \right| \\
&\quad + \left| e_k^{[n_m]}(\lambda^m \bar{r},\tau) - e_k^{[\infty]}(\lambda^m \bar{r},\tau) \right| \\
&\overset{(8)}{=} \underbrace{\left| G_m \mathcal{T}^m(\mathbf{v}_k^{[n_0]})(\bar{r},\tau) - G_m A^m(\mathbf{v}_k^{[n_m]})(\bar{r},\tau) \right|}_{\text{Both } \mathcal{T}^m \mathbf{v}_k^{[n_0]} \text{ and } A^m \mathbf{v}_k^{[n_m]} \text{ have valence } n_m;\ G_m \text{ is linear}} \\
&\quad + \underbrace{\lambda_k^m}_{\mathrm{O}(\lambda^m)} \underbrace{\left| e_k^{[n_m]}(\bar{r},\tau) - e_k^{[\infty]}(\bar{r},\tau) \right|}_{\text{Lem. 3: } \mathrm{O}\left(\frac{1}{n_m^2}\right) = \mathrm{O}\left(\frac{1}{4^m}\right)} \\
&= \left| G_m(\mathcal{T}^m(\mathbf{v}_k^{[n_0]}) - A^m(\mathbf{v}_k^{[n_m]}))(\bar{r},\tau) \right| + \mathrm{O}\left(\frac{1}{8^m}\right).
\end{aligned}
$$

By (26), for $h \in \mathbb{Z}_6$, $\mathbf{p}_h = \delta_{hk}$ when $\mathbf{q} = \mathbf{v}_k^{[n_0]}$ or $\mathbf{q} = \mathbf{v}_k^{[n_m]}$. Therefore the first six eigencoefficients of $\mathbf{q} = \mathbf{v}_k^{[n_0]}$ and $\mathbf{q} = \mathbf{v}_k^{[n_m]}$ match and $\mathcal{T}^m(\mathbf{v}_k^{[n_0]})$ and $A^m(\mathbf{v}_k^{[n_m]})$ in (30) and (28) differ by $\mathrm{o}(\mu^m)$. Therefore $E = \mathrm{o}(\mu^m)$. □

Since Lemma 3 shows that $e_k^{[\infty]}(r,\tau)$ of RTS reproduces the second-order Taylor basis, Lemma 4 implies that $f_k(r,\tau)$, too, reproduces this basis once it reaches the pole at $m \to \infty$.

5.5 Curvature continuity of C^2PS surfaces

We can now give the second-order Taylor expansion at the pole, proving curvature continuity of C^2PS.

Theorem 1. *For generic data* $\mathbf{q}$*, C^2PS surfaces are C^2 at the pole.*

Proof. As in (25), a polar configuration $\mathbf{q}^0$ of valence n_0 can be written as the following linear combination of the eigenvectors, $\mathbf{v}_k^{[n_0]}$, $k \in \mathbb{Z}_{6n_0}$.

$$
\mathbf{q}_{ij}^0 = \sum_k^{6n_0} \mathbf{p}_k \, (\mathbf{v}_k^{[n_0]})_{ij} \quad \Rightarrow \quad \mathbf{x}^{\mathrm{C^2PS}}(r,\tau) = \sum_k^{6n_0} \mathbf{p}_k \, f_k(r,\tau).
$$

We examine the sequence

$$
\mathbf{x}^{\mathrm{C^2PS}}(r,\tau)\big|_{r \in [2\lambda^m, 4\lambda^m]} \overset{(8)}{=} \left(G_m \mathcal{T}^m \mathbf{q}^0\right)(r,\tau)
$$

of spline rings that approach the pole. Since $\frac{r}{\lambda^m} \in [2,4]$, $\frac{r}{\lambda^m}$ is bounded away from 0 and ∞, so that $\mathrm{o}(\mu^m) = \mathrm{o}\left(\lambda^{2m}\right) = \mathrm{o}\left((\frac{r}{\lambda^m})^2 \lambda^{2m}\right) = \mathrm{o}\left(r^2\right)$. Thus, for $r \in [2\lambda^m, 4\lambda^m]$,

$$
\begin{aligned}
\mathbf{x}^{\mathrm{C^2PS}}(r,\tau) &= \sum_k^{6n_0} \mathbf{p}_k \, f_k(r,\tau) \overset{\text{Lem. 4}}{=} \sum_k^{6n_0} \mathbf{p}_k \, e_k^{[\infty]}(r,\tau) + \mathrm{o}(\mu^m) \\
&= \mathbf{p}_0 \, e_0^{[\infty]}(r,\tau) + \left(\mathbf{p}_1 \, e_1^{[\infty]}(r,\tau) + \mathbf{p}_2 \, e_2^{[\infty]}(r,\tau)\right) \\
&\quad + \left(\mathbf{p}_3 \, e_3^{[\infty]}(r,\tau) + \mathbf{p}_4 \, e_4^{[\infty]}(r,\tau) + \mathbf{p}_5 \, e_5^{[\infty]}(r,\tau)\right) \\
&\quad + \sum_{k=6}^{6n_0} \mathbf{p}_k \, e_k^{[\infty]}(r,\tau) + \mathrm{o}\left(r^2\right) \\
&\overset{\text{Lem. 2 \& 3}}{=} \mathbf{p}_0 + r\left(\mathbf{p}_1 c_\tau + \mathbf{p}_2 s_\tau\right) + r^2\left(\mathbf{p}_3 + \mathbf{p}_4 c_{2\tau} + \mathbf{p}_5 s_{2\tau}\right) + \mathrm{o}\left(r^2\right)
\end{aligned}
$$

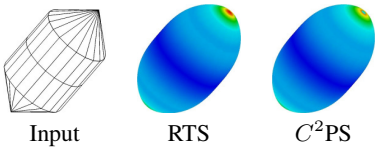

Figure 12: Polar configuration of valence 20. *Limit surfaces and Gaussian curvature distributions (dark blue is near-zero curvature) of RTS and C^2PS are similar for large polar valences.*

Restricting $\sqrt{x^2+y^2}$ to $[2\lambda^m, 4\lambda^m]$, a change to Cartesian coordinates

$$
(rc_\tau, rs_\tau) \to (x,y), \quad \mathbf{x}^{\mathrm{C^2PS}}(r,\tau) \to \overline{\mathbf{x}}^{\mathrm{C^2PS}}(x,y)
$$

yields

$$
\begin{aligned}
\overline{\mathbf{x}}^{\mathrm{C^2PS}}(x,y) = \mathbf{p}_0 &+ \mathbf{p}_1 x + \mathbf{p}_2 y + \mathbf{p}_3(x^2+y^2) \\
&+ \mathbf{p}_4(x^2-y^2) + \mathbf{p}_5(2xy) + \mathrm{o}\left(x^2+y^2\right),
\end{aligned} \tag{32}
$$

an explicit second-order expansion at the pole when $m \to \infty$. Therefore the construction is C^2. □

That is, $\mathbf{p}_0$ is the limit point, $\mathbf{p}_1$ and $\mathbf{p}_2$ span the tangent plane and $\mathbf{p}_3$, $\mathbf{p}_4$ and $\mathbf{p}_5$ determine the quadratic variation at the pole.

6 Results

Figure 11 compares C^2 polar Jet subdivision [Karčiauskas et al. 2006], RTS, and C^2PS. We do not compare with BPS [Karčiauskas and Peters 2007c] since its surfaces appear qualitatively no different from RTS for finite valence. To avoid curvature fluctuations in the first and second spline rings as observed in Figure 11(a-b), the refined 2-link for RTS and C^2PS is computed by uniform (bi-)3 refinement for the first subdivision step (Figure 11(c-e)). For RTS, this is equivalent to applying one step of BPS.

Side-by-side comparison reveals the n-sidedness of Jet subdivision and RTS surfaces in the periodic direction. C^2PS distributes the curvature without preferred *periodic* direction. In the *radial* direction, both Jet subdivision and C^2PS distribute the curvature more evenly than RTS, yielding rounder silhouettes. In short, the bi-3 C^2PS compares favorably with Jet subdivision, although Jet subdivision uses degree $(6,5)$ patches and is more complex to implement.

Figure 12 confirms that RTS and C^2PS limit surfaces are similar for high valences. In some constructions, curvature continuity comes at the cost of macroscopic shape deterioration, even though the microscopic shape is improved. Figure 13 tests C^2PS against various challenging configurations. The smooth highlight lines attest to the surface quality in the vicinity of the pole, even on higher-order saddles.

7 Summary, Limitation, and Future Work

We introduced C^2PS, a subdivision algorithm that produces bi-3 polar caps that are C^2 also at the pole. The algorithm employs increasing valence but stationary weights for a given valence, making it easy to implement and naturally capable of handling high polar valences. We formally analyzed C^2PS with the help of an auxiliary C^2 stationary scheme (RTS with $n \to \infty$) and were able to obtain the explicit quadratic Taylor expansion (32). This allows computing any intrinsic properties of the surface at the pole. Particularly,

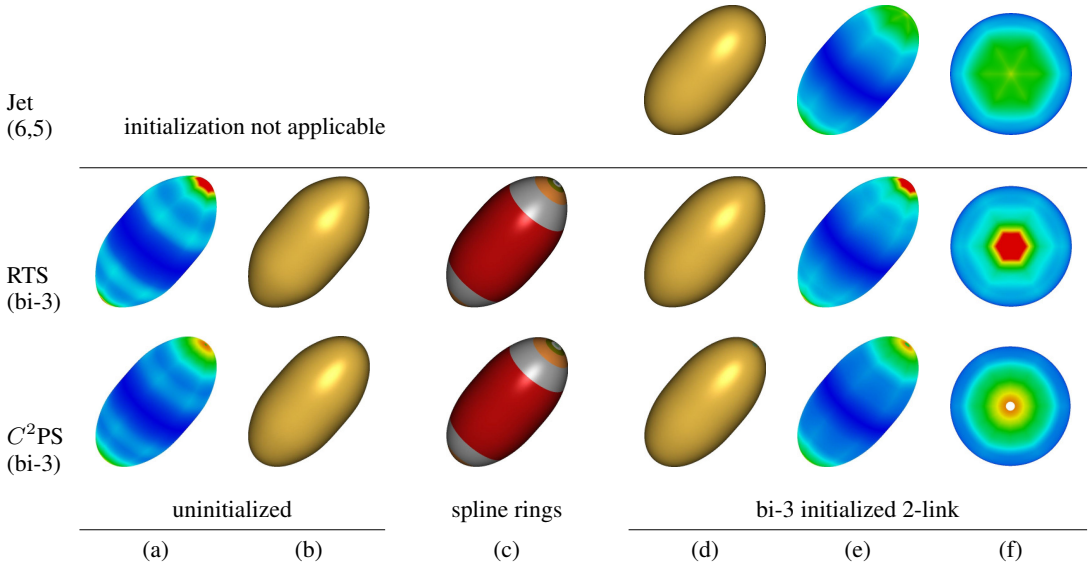

Figure 11: Comparison *of Jet subdivision, RTS, and C^2PS. (c) Spline surface rings of the limit surfaces (b, d) and Gauss curvature (a, e) where dark blue indicates zero Gauss curvature. Initialization by applying uniform bi-3 subdivision for the* 2*-link in the first step (c, d, e) yields a more monotone curvature distribution and smoother silhouette than direct application (*left two*). (f) Gauss curvature of Jet subdivision and RTS reveal the n-sidedness of the input.*

it provides the limit point $\mathbf{p}_0$ of the polar vertex explicitly via (27). The limit formulas of 1-link vertices are computed by subdividing once and applying the standard rule for evaluating a bi-3 spline at a knot-line crossing.

We note for implementation that vertex/facet lists or half-edge data structures scale to arbitrary valence. Therefore, we need not be concerned that the mesh size near the polar vertex doubles as the mesh refines at the same rate as for Catmull-Clark subdivision.

Clearly the main limitation of C^2PS is its restriction to polar configurations. Figure 14 shows that inserting 5-valent extraordinary vertices (Figure 14(a)) or pentagons (Figure 14(c)) reduces Catmull-Clark extraordinary vertices to polar configurations. Special rules for valence 5 can then yield a globally C^2 subdivision surface. However, the number of extraordinary regions is increased and we have not yet explored under what conditions such rules result in good shape.

One concern with standard local mesh averaging subdivision is a lack of curvature information near extraordinary vertices. C^2PS is a (first) local mesh averaging subdivision that provides this information explicitly. In fact, the framework can in principle yield higher-order, e.g. a C^3 bi-4 polar scheme. To apply the proof technique, we need to establish $\mathrm{o}(r^3) = \mathrm{o}(\lambda^{3m})$ bounds on the deviation from an auxiliary C^3 subdivision algorithm. The key technical challenge here is that the deviation contributed by piecewise-linear approximations to cosines and sines in the Appendix and the proof of Lemma 3 cannot be reduced simply by choosing a higher-degree construction.

Acknowledgements

We thank David Groisser, Kestutis Karčiauskas, and the SIGGRAPH reviewers for their constructive feedback This work was supported by the National Science Foundation Grant 0728797.

References

CATMULL, E., AND CLARK, J. 1978. Recursively generated B-spline surfaces on arbitrary topological meshes. *Computer Aided Design 10*, 350–355.

CHOI, Y.-J., LEE, Y. J., YOON, J., LEE, B.-G., AND KIM, Y. J. 2006. A new class of non-stationary interpolatory subdivision schemes based on exponential polynomials. In *Geometric Modeling and Processing*, 563–570.

FARIN, G. 1997. *Curves and Surfaces for Computer-Aided Geometric Design: A Practical Guide*, fourth ed. Academic Press, San Diego, CA, USA.

KARČIAUSKAS, K., MYLES, A., AND PETERS, J. 2006. A C^2 polar jet subdivision. In *SGP '06: Proceedings of the Fourth Eurographics Symposium on Geometry Processing*, Eurographics Association, Aire-la-Ville, Switzerland, Switzerland, 173–180.

KARČIAUSKAS, K., AND PETERS, J. 2007. Concentric tessellation maps and curvature continuous guided surfaces. *Comput. Aided Geom. Des. 24*, 2, 99–111.

KARČIAUSKAS, K., AND PETERS, J. 2007. On the curvature of guided surfaces. Tech. rep., University of Florida CISE, REP-2007-430, Gainesville, FL, USA.

KARČIAUSKAS, K., AND PETERS, J. 2007. Bicubic polar subdivision. *ACM Trans. Graph. 26*, 4, 14.

KARČIAUSKAS, K., AND PETERS, J. 2008. On the curvature of guided surfaces. *Comput. Aided Geom. Des. 25*, 2, 69–79.

LEVIN, A. 2006. Modified subdivision surfaces with continuous curvature. In *SIGGRAPH '06: ACM SIGGRAPH 2006 Papers*, ACM Press, New York, NY, USA, 1035–1040.

LOOP, C. T., AND SCHAEFER, S. 2008. G^2 tensor product splines over extraordinary vertices. *Computer Graphics Forum (Proceedings of 2008 Symposium on Geometry Processing) 27*, 5, 1373–1382.

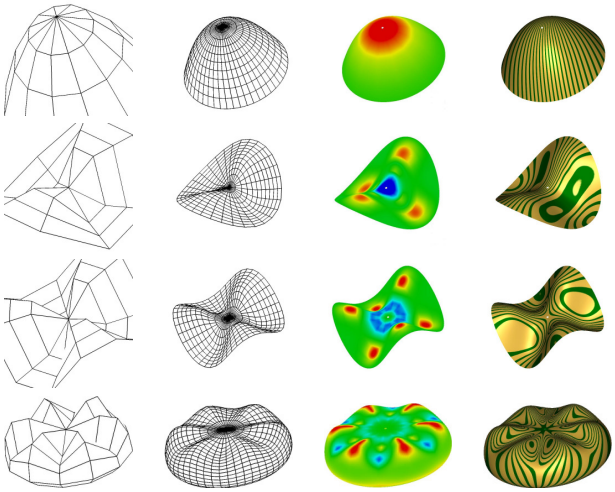

Figure 13: Shape gallery *demonstrating that C^2PS can preserve shape. (a) Input, (b) twice subdivided mesh, (c) Gaussian curvature of limit surface, and (d) highlight lines. The* green *range straddles Gauss zero curvature, while negative curvature is* blue *and positive is* red*. Larger* blue *or* red *areas result from saturation in normalization.*

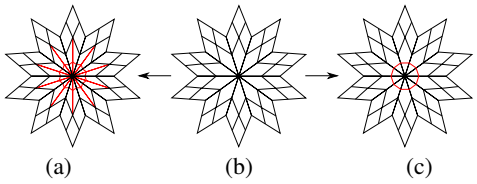

Figure 14: Conversion *of (b) an n-valent Catmull-Clark extraordinary vertex to (a) a $2n$-valent polar configuration and n 5-valent extraordinary vertices, respectively (c) a n-valent polar configuration and n pentagons.*

LOOP, C. T. 2004. Second order smoothness over extraordinary vertices. In *SGP '04: Proceedings of the 2004 Eurographics/ACM SIGGRAPH Symposium on Geometry Processing*, ACM, New York, NY, USA, 165–174.

LUTTERKORT, D., AND PETERS, J. 2001. Tight linear envelopes for splines. *Numerische Mathematik 89*, 4 (Oct), 735–748.

MORIN, G., WARREN, J. D., AND WEIMER, H. 2001. A subdivision scheme for surfaces of revolution. *Comput. Aided Geom. Des. 18*, 5, 483–502.

MYLES, A., KARČIAUSKAS, K., AND PETERS, J. 2008. Pairs of bi-cubic surface constructions supporting polar connectivity. *Comput. Aided Geom. Des. 25*, 8, 621–630.

MYLES, A. 2008. *Curvature-continuous bicubic subdivision surfaces for polar configurations*. PhD thesis, University of Florida, Gainesville, Florida.

PETERS, J., AND REIF, U. 2008. *Subdivision Surfaces*. Geometry and Computing, Vol. 3. Springer-Verlag New York, Inc., New York, NY, USA, Apr.

PETERS, J. 2002. C^2 free-form surfaces of degree (3,5). *Comput. Aided Geom. Des. 19*, 2, 113–126.

PRAUTZSCH, H., AND REIF, U. 1999. Degree estimates for C^k-piecewise polynomial subdivision surfaces. *Advances in Computational Mathematics 10*, 2, 209–217.

PRAUTZSCH, H., AND REIF, U. 1999. Necessary conditions for subdivision surfaces. *Advances in Computational Mathematics 10*, 209–217.

PRAUTZSCH, H., AND UMLAUF, G. 1998. A G^2-subdivision algorithm. In *Geometric Modeling, Dagstuhl, Germany, 1996*, Springer-Verlag, London, UK, 217–224.

PRAUTZSCH, H., BOEHM, W., AND PALUSZNY, M. 2002. *Bezier and B-Spline Techniques*. Springer-Verlag New York, Inc., Secaucus, NJ, USA.

PRAUTZSCH, H. 1997. Freeform splines. *Comput. Aided Geom. Des. 14*, 3, 201–206.

REIF, U. 1998. TURBS—topologically unrestricted rational B-splines. *Constructive Approximation. An International Journal for Approximations and Expansions 14*, 1, 57–77.

WALLNER, J., AND DYN, N. 2005. Convergence and C^1 analysis of subdivision schemes on manifolds by proximity. *Comput. Aided Geom. Des. 22*, 7, 593–622.

YING, L., AND ZORIN, D. 2004. A simple manifold-based construction of surfaces of arbitrary smoothness. *ACM Trans. Graph. 23*, 3 (Aug.), 271–275.

ZHANG, H., AND WANG, G. 2002. Semi-stationary subdivision operators in geometric modeling. *Progress in National Science 12*, 10, 772–776.

ZORIN, D. 2006. Constructing curvature-continuous surfaces by blending. In *SGP '06: Proceedings of the Fourth Eurographics Symposium on Geometry Processing*, Eurographics Association, Aire-la-Ville, Switzerland, Switzerland, 31–40.

ZULTI, A., LEVIN, A., LEVIN, D., AND TEICHER, M. 2006. C^2 subdivision over triangulations with one extraordinary point. *Comput. Aided Geom. Des. 23*, 2, 157–178.

A Reformulation of C^2PS in eigenspace

We expand C^2PS in terms of its eigencoefficients to prove in Section A.1 that $\mathbf{p}_k^m = \lambda_k^m \mathbf{p}_k$. In Section A.2, we use this to prove the crucial expansion estimate (30).

In this Appendix, $\mathbf{q}^m$ is generated by C^2PS. That is, $\mathbf{q}^m := \mathcal{T}^m \mathbf{q}$ and $\mathbf{p}_k^m := \mathbf{w}_k^{\mathrm{T}} \mathbf{q}^m$. For a degree 3 spline with knots $\mathbf{t} := [t_0, t_1, \ldots, t_{n+3}]$ and control points $\mathbf{b} := [b_0, b_1, \ldots, b_{n-1}]$, the *Greville abscissa* $t_i^* := \frac{1}{3}(t_{i+1}+t_{i+2}+t_{i+3})$ is the domain parameter associated with each control point b_i. We index with Greville abscissa, e.g. $\mathbf{q}_{i,[j/n_m]}^m := \mathbf{q}_{ij}^m$, since $\mathbf{q}^m$ defines a spline surface ring whose Greville abscissa sequence in the periodic direction is $\frac{1}{n_m}\mathcal{Z}_{n_m}$. Also, $\mathbb{F}_n := \frac{1}{n}\mathbb{Z}_n \subset \mathbb{R}_1$ and,

for sets S, $\sum_{\xi}^{S}$ denotes $\sum_{\xi \in S}$.

A.1 Scaling of eigencoefficients

Lemma 5. *For C^2PS and $k \in \mathbb{Z}_6$, $\mathbf{p}_k^m = \lambda_k^m \mathbf{p}_k$.*

Proof. Since the other cases are alike, we show only the case $k = 1$. The case $m = 0$ of our proof by induction is trivially true. For the inductive step, we assume $\mathbf{p}_1^m = \lambda_1^m \mathbf{p}_1$ and show that this scaling holds for $\mathbf{p}_1^{m+1}$ as well.

By the addition rule for sine and cosine and the orthogonality of the discrete Fourier basis,

$$\frac{1}{2n}\sum_{\gamma}^{\mathbb{F}_{2n}} c_{a_1(\gamma-\tau)} \frac{1}{n}\sum_{\xi}^{\mathbb{F}_n} c_{a_2(\xi-\gamma)} \mathbf{q}_{i,[\xi]} = \begin{cases} \frac{1}{n}\sum_{\xi}^{\mathbb{F}_n} \mathbf{q}_{i,[\xi]} & \text{if } a_1 = a_2 = 0 \\ \frac{1}{2n}\sum_{\xi}^{\mathbb{F}_n} c_{a_1(\xi-\tau)} \mathbf{q}_{i,[\xi]} & \text{if } a_1 = \pm a_2 \neq 0 \\ 0 & \text{otherwise} \end{cases} \tag{33}$$

$$\text{and } \frac{1}{2n}\sum_{\gamma}^{\mathbb{F}_{2n}} s_{a_1(\gamma-\tau)} \frac{1}{n}\sum_{\xi}^{\mathbb{F}_n} c_{a_2(\xi-\gamma)} \mathbf{q}_{i,[\xi]} = \begin{cases} \frac{\pm 1}{2n}\sum_{\xi}^{\mathbb{F}_n} s_{a_1(\xi-2)} \mathbf{q}_{i,[\xi]} & \text{if } a_1 = \pm a_2 \neq 0 \\ 0 & \text{otherwise,} \end{cases}$$

so that

$$\begin{aligned} \mathbf{p}_1^{m+1} &\overset{(27)}{=} \frac{2}{n_{m+1}} \sum_{\gamma}^{\mathbb{F}_{2n_m}} c_\gamma \mathbf{q}_{1,[\gamma]}^{m+1} \\ &\overset{(2)}{=} \frac{2}{2n_m}\sum_{\gamma}^{\mathbb{F}_{2n_m}} c_\gamma \left(\frac{1}{2}\mathbf{q}_{00}^m + \frac{1}{n_m}\sum_{\xi}^{\mathbb{F}_{n_m}} \left(\frac{1}{2} + c_{\xi-\gamma} + \frac{1}{2}c_{2(\xi-\gamma)}\right) \mathbf{q}_{1,[\xi]}^m \right) \\ &\overset{(33)}{=} \frac{2}{2n_m}\sum_{\xi}^{\mathbb{F}_{n_m}} c_\xi \mathbf{q}_{1,[\xi]}^m = \frac{1}{2}\mathbf{p}_1^m = \lambda_1 \mathbf{p}_1^m = \lambda_1^{m+1}\mathbf{p}_1, \end{aligned}$$

completes the induction step. □

A.2 C^2PS in terms of the eigencoefficients

Here, we establish (30). A check mark (✔) indicates that one of these equations has been proved. We express $\mathbf{q}_{00}^m$ and $\mathbf{q}_{1j}^m$ in terms of the eigencoefficients:

$$\begin{aligned} \mathbf{q}_{00}^{m+1} &\overset{(1)}{=} \frac{3}{4}\mathbf{q}_{00}^m + \frac{1}{4n_m}\sum_{\xi}^{\mathbb{F}_{n_m}} \mathbf{q}_{1,[\xi]}^m \overset{(27)}{=} \mathbf{p}_0^m - \frac{1}{12}\mathbf{p}_3^m \\ \boxed{\checkmark} &= \mathbf{p}_0 - \frac{\mu^m}{12}\mathbf{p}_3 = \mathbf{p}_0 - \frac{\mu^{m+1}}{3}\mathbf{p}_3 \end{aligned} \tag{34}$$

$$\begin{aligned} \mathbf{q}_{1,[\tau]}^{m+1} &\overset{(2)}{=} \frac{1}{2}\mathbf{q}_{00}^m + \frac{1}{n_m}\sum_{\xi}^{\mathbb{F}_{n_m}} \left(\frac{1}{2} + c_{\xi-\tau} + \frac{1}{2}c_{2(\xi-\tau)}\right) \mathbf{q}_{1,[\xi]}^m \\ &\overset{\substack{\text{add. rule}\\ \text{for cos}}}{\overset{(27)}{=}} \mathbf{p}_0^m + \frac{1}{2}(\mathbf{p}_1^m c_\tau + \mathbf{p}_2^m s_\tau) + \frac{1}{6}(\mathbf{p}_3^m + \mathbf{p}_4^m c_{2\tau} + \mathbf{p}_5^m s_{2\tau}) \\ &\overset{\text{Lemma 5}}{=} \mathbf{p}_0 + \lambda^{m+1}(\mathbf{p}_1 c_\tau + \mathbf{p}_2 s_\tau) \\ \boxed{\checkmark} &\quad + \frac{2\mu^{m+1}}{3}(\mathbf{p}_3 + \mathbf{p}_4 c_{2\tau} + \mathbf{p}_5 s_{2\tau}), \end{aligned} \tag{35}$$

and observe

$$\begin{aligned} \mathbf{q}_{2,[\tau]}^m &\overset{\substack{(3)\\(27)}}{=} \frac{11}{12}\tilde{\mathbf{q}}_{1,[\tau]}^{m-1} + \frac{1}{12}\tilde{\mathbf{q}}_{2,[\tau]}^{m-1} - \frac{1}{6}(\mathbf{p}_1^{m-1} c_\tau + \mathbf{p}_2^{m-1} s_\tau) \\ &\overset{\text{Lemma 5}}{=} \frac{11}{12}\tilde{\mathbf{q}}_{1,[\tau]}^{m-1} + \frac{1}{12}\tilde{\mathbf{q}}_{2,[\tau]}^{m-1} - \frac{\lambda^m}{3}(\mathbf{p}_1 c_\tau + \mathbf{p}_2 s_\tau). \end{aligned} \tag{36}$$

The expressions for the four outer links $\mathbf{q}_2$, $\mathbf{q}_3$, $\mathbf{q}_4$, and $\mathbf{q}_5$ are more complex due to the degree-3 subdivision (5) in the periodic direction. Fortunately, only the dominant terms are needed and we can use the fact that every point on a degree 3 spline is an affine combination of the four B-spline control points parametrically closest to it. We capture this formally by defining an equivalence class of affine combinations.

Definition 3 ($\mathrm{aff}^4_{[\gamma]}$)**.** *Let $\mathbf{u} := \left[\mathbf{u}_{\left[\frac{0}{n}\right]}, \ldots, \mathbf{u}_{\left[\frac{n-1}{n}\right]}\right]$ be a vector of n B-spline control points (indexed by their Greville abscissae $\frac{1}{n}$ apart) of a periodic uniform degree 3 spline with knot sequence $\frac{1}{n}\mathcal{Z}_n$. The equivalence class $\mathrm{aff}^4_{[\gamma]}(\mathbf{u})$ of all local affine combinations centered at γ is defined as*

$$\mathrm{aff}^4_{[\gamma]}(\mathbf{u}) := \left\{ \sum_g^4 u_g \mathbf{u}_{[\gamma_g]} \;\middle|\; \begin{array}{l} \sum_g^4 u_g = 1, \;\; \sum_g^4 u_g \gamma_g = \gamma, \\ \text{and } \mathbf{u}_{[\gamma_0]}, \ldots, \mathbf{u}_{[\gamma_3]} \text{ are the 4} \\ \text{control points whose Greville} \\ \text{abscissae } \gamma_g \text{ are closest to} \\ \gamma, \text{ or have weight } u_g = 0 \text{ if} \\ \text{they tie for fourth place.} \end{array} \right\}$$

Since adjacent Greville abscissae differ by $\frac{1}{n}$, the weights in $\mathrm{aff}^4_{[\gamma]}(\mathbf{u})$ are such that $|\gamma_g - \gamma| < \frac{2}{n}$ if $u_g \neq 0$.

Recall from (5) that the control points in each subdivided i-link $\tilde{\mathbf{q}}_i^m$ are affine combinations of control points in the i-link $\mathbf{q}_i^m$ under degree 3 B-spline rules. Since refinements on $\mathbf{u}$ remain in $\mathrm{aff}^4_{[\gamma]}(\mathbf{u})$, we can estimate the multitude of affine combinations arising in the analysis of C^2PS in terms of affine combinations of trigonometric functions.

Lemma 6. *If $\mathbf{u} := [\mathrm{op}_k(\frac{g}{n})]_{g\in\mathbb{Z}_n}$, then for all $\tilde{\mathbf{u}}_{[\gamma]} := \sum_g^4 u_g \mathbf{u}_{[\gamma_g]} \in \mathrm{aff}^4_{[\gamma]}(\mathbf{u})$,*

$$\tilde{\mathbf{u}}_{[\gamma]} = \mathrm{op}_k(\gamma) + \mathrm{O}\left(\frac{\alpha_k^2}{n^2}\right).$$

Proof.
Case 1: $\alpha_k = 0$ (i.e. $\mathrm{op}_k(\gamma) = c_{0\gamma} = 1$)
For $\mathbf{u} = [1]_{g\in\mathbb{Z}_n}$, $\tilde{\mathbf{u}}_{[\gamma]} = \sum_g^4 u_g \underbrace{\mathbf{u}_{[\gamma_g]}}_{1} = \sum_g^4 u_g = 1 = \mathrm{op}_k(\gamma)$.

Case 2: $\mathbf{u}_\gamma = c_{\alpha_k\gamma}$, $\alpha_k \neq 0$

$$\begin{aligned}
\tilde{\mathbf{u}}_{[\gamma]} &= \sum_g^4 u_g c_{\alpha_k\gamma_g} \quad = \quad \sum_g^4 u_g c_{\alpha_k(\gamma_g-\gamma)+\alpha_k\gamma} \\
&= \sum_g^4 u_g \left(c_{\alpha_k(\gamma_g-\gamma)}c_{\alpha_k\gamma} - s_{\alpha_k(\gamma_g-\gamma)}s_{\alpha_k\gamma}\right) \quad \begin{smallmatrix}\text{Taylor expan. \&}\\ |\gamma_g-\gamma| = \mathrm{O}\left(\frac{1}{n}\right)\end{smallmatrix} \\
&= \sum_g^4 u_g \underbrace{\left(1+\mathrm{O}\left(\frac{\alpha_k^2}{n^2}\right)\right)}_{\text{from } c_{\alpha_k(\gamma_g-\gamma)}} c_{\alpha_k\gamma} - u_g \underbrace{\left(\alpha_k(\gamma_g-\gamma)+\mathrm{O}\left(\frac{\alpha_k^3}{n^3}\right)\right)}_{\text{from } s_{\alpha_k(\gamma_g-\gamma)}} s_{\alpha_k\gamma} \\
&= c_{\alpha_k\gamma}\cancel{\sum_g^4 u_g}^{1} + \alpha_k s_{\alpha_k\gamma}\cancel{\sum_g^4 u_g(\gamma_g-\gamma)}^{0} + \mathrm{O}\left(\frac{\alpha_k^2}{n^2}\right) \\
&= c_{\alpha_k\gamma} + \mathrm{O}\left(\frac{\alpha_k^2}{n^2}\right),
\end{aligned}$$

as claimed.

Case 3: $\mathbf{u}_\gamma = -s_{\alpha_k\gamma}$, $\alpha_k \neq 0$

Estimates analogous to Case 2 prove $\tilde{\mathbf{u}}_{[\gamma]} = -s_{\alpha_k\gamma} + \mathrm{O}\left(\frac{\alpha_k^2}{n^2}\right)$. □

Equipped with Lemma 6, we can now estimate $\mathbf{q}^m_{2,[\tau]}$ by describing $\mathrm{aff}^4_{[\tau]}(\mathbf{q}_2^m) \ni \mathbf{q}^m_{2,[\tau]}$ in terms of $\mathbf{p}_{k\in\mathbb{Z}_6}$. The bound $\mathrm{O}\left(\frac{\alpha_k^2}{n_m^2}\right)$ on the terms not explicitly written in terms of $\mathbf{p}_k$ simplifies to $\mathrm{O}\left(\frac{1}{4^m}\right)$ since $\alpha_k \in \{0,1,2\}$ in the relevant cases and $n_m = n_0 2^m$. For each affine combination $\tilde{\mathbf{u}}^{\mathbf{q}_1^m}_{[\tau]} \in \mathrm{aff}^4_{[\tau]}(\mathbf{q}_1^m)$ of control points $\mathbf{q}_1^m$,

$$\begin{aligned}
\tilde{\mathbf{u}}^{\mathbf{q}_1^m}_{[\tau]} &\underset{\text{Lem 6}}{\overset{(35)}{=}} \mathbf{p}_0 + \lambda^m\left(\mathbf{p}_1\left(c_\tau + \mathrm{O}\left(\frac{1}{4^m}\right)\right) + \mathbf{p}_2\left(s_\tau + \mathrm{O}\left(\frac{1}{4^m}\right)\right)\right) \\
&+ \frac{2\mu^m}{3}\left(\mathbf{p}_3 + \mathbf{p}_4\left(c_{2\tau} + \mathrm{O}\left(\frac{1}{4^m}\right)\right) + \mathbf{p}_5\left(s_{2\tau} + \mathrm{O}\left(\frac{1}{4^m}\right)\right)\right) \\
&= \mathbf{p}_0 + \lambda^m(\mathbf{p}_1 c_\tau + \mathbf{p}_2 s_\tau) + \frac{2\mu^m}{3}(\mathbf{p}_3 + \mathbf{p}_4 c_{2\tau} + \mathbf{p}_5 s_{2\tau}) + \mathrm{O}\left(\frac{1}{8^m}\right).
\end{aligned} \tag{37}$$

For each $\tilde{\mathbf{u}}^{\mathbf{q}_2^m}_{[\tau]} \in \mathrm{aff}^4_{[\tau]}(\mathbf{q}_2^m)$, there exist $\tilde{\mathbf{u}}^{\mathbf{q}_1^{m-1}}_{[\tau]} \in \mathrm{aff}^4_{[\tau]}(\mathbf{q}_1^{m-1})$ and $\tilde{\mathbf{u}}^{\mathbf{q}_2^{m-1}}_{[\tau]} \in \mathrm{aff}^4_{[\tau]}(\mathbf{q}_2^{m-1})$ so that

$$\begin{aligned}
\tilde{\mathbf{u}}^{\mathbf{q}_2^m}_{[\tau]} &\underset{\text{Lem 6}}{\overset{(36)}{=}} \frac{11}{12}\tilde{\mathbf{u}}^{\mathbf{q}_1^{m-1}}_{[\tau]} + \frac{1}{12}\tilde{\mathbf{u}}^{\mathbf{q}_2^{m-1}}_{[\tau]} - \frac{\lambda^m}{3}\left(\mathbf{p}_1 c_\tau + \mathbf{p}_2 s_\tau + \mathrm{O}\left(\frac{1}{4^m}\right)\right) \\
&\underset{\text{Lem 6}}{\overset{(37)}{=}} \frac{11}{12}\left(\mathbf{p}_0 + \lambda^{m-1}(\mathbf{p}_1 c_\tau + \mathbf{p}_2 s_\tau)\right. \\
&\qquad \left. + \frac{2\mu^{m-1}}{3}(\mathbf{p}_3 + \mathbf{p}_4 c_{2\tau} + \mathbf{p}_5 s_{2\tau}) + \mathrm{O}\left(\frac{1}{8^{m-1}}\right)\right) \\
&\qquad + \frac{1}{12}\tilde{\mathbf{u}}^{\mathbf{q}_2^{m-1}}_{[\tau]} - \frac{\lambda^m}{3}(\mathbf{p}_1 c_\tau + \mathbf{p}_2 s_\tau) + \mathrm{O}\left(\frac{1}{8^m}\right) \\
&= \frac{11}{12}\mathbf{p}_0 + \frac{5}{3}\lambda^m(\mathbf{p}_1 c_\tau + \mathbf{p}_2 s_\tau) \\
&\quad + \frac{22}{9}\mu^m(\mathbf{p}_3 + \mathbf{p}_4 c_{2\tau} + \mathbf{p}_5 s_{2\tau}) + \mathrm{O}\left(\frac{1}{8^m}\right) + \frac{1}{12}\tilde{\mathbf{u}}^{\mathbf{q}_2^{m-1}}_{[\tau]}.
\end{aligned} \tag{38}$$

Equation (38) describes the set $\mathrm{aff}^4_{[\tau]}(\mathbf{q}_2^m)$ recursively in terms of $\mathrm{aff}^4_{[\tau]}(\mathbf{q}_2^{m-1})$. Expanding the recursion reveals geometric series such that, for each $\tilde{\mathbf{u}}^{\mathbf{q}_2^m}_{[\tau]} \in \mathrm{aff}^4_{[\tau]}(\mathbf{q}_2^m)$, there exists $\tilde{\mathbf{u}}^{\mathbf{q}_2^0}_{[\tau]} \in \mathrm{aff}^4_{[\tau]}(\mathbf{q}_2^0)$ with

$$\begin{aligned}
\tilde{\mathbf{u}}^{\mathbf{q}_2^m}_{[\tau]} &= \frac{11}{12}\left(\sum_h^m \frac{1}{12^h}\right)\mathbf{p}_0 + \frac{5}{3}\left(\sum_h^m \frac{\lambda^{m-h}}{12^h}\right)(\mathbf{p}_1 c_\tau + \mathbf{p}_2 s_\tau) \\
&\quad + \frac{22}{9}\left(\sum_h^m \frac{\mu^{m-h}}{12^h}\right)(\mathbf{p}_3 + \mathbf{p}_4 c_{2\tau} + \mathbf{p}_5 s_{2\tau}) \\
&\quad + \mathrm{O}\left(\sum_h^m \frac{1}{8^{m-h}12^h}\right) + \frac{1}{12^m}\tilde{\mathbf{u}}^{\mathbf{q}_2^0}_{[\tau]} \\
&= \left(1-\frac{1}{12^m}\right)\mathbf{p}_0 + 2\lambda^m\left(1-\frac{1}{6^m}\right)(\mathbf{p}_1 c_\tau + \mathbf{p}_2 s_\tau) \\
&\quad + \mu^m\frac{11}{3}\left(1-\frac{1}{3^m}\right)(\mathbf{p}_3 + \mathbf{p}_4 c_{2\tau} + \mathbf{p}_5 s_{2\tau}) \quad \begin{smallmatrix}\text{geom.}\\ \text{series}\end{smallmatrix} \\
&\quad + \mathrm{O}\left(\frac{3}{8^m}\left(1-\left(\frac{2}{3}\right)^m\right)\right) + \frac{1}{12^m}\tilde{\mathbf{u}}^{\mathbf{q}_2^0}_{[\tau]} \\
&= \mathbf{p}_0 + 2\lambda^m(\mathbf{p}_1 c_\tau + \mathbf{p}_2 s_\tau) \\
&\quad + \frac{11\mu^m}{3}(\mathbf{p}_3 + \mathbf{p}_4 c_{2\tau} + \mathbf{p}_5 s_{2\tau}) + \mathrm{O}\left(\frac{1}{8^m}\right). \quad \boxed{\checkmark}
\end{aligned} \tag{39}$$

Since $\mathbf{q}^m_{2,[\tau]} \in \mathrm{aff}^4_{[\tau]}(\mathbf{q}_2^m)$, it too is described by (39), proving (30) for $i = 2$.

The non-recursive derivation for $\tilde{\mathbf{u}}^{\mathbf{q}_3^m}_{[\tau]} \in \mathrm{aff}^4_{[\tau]}(\mathbf{q}_3^m)$, is far simpler and easily yields formulas for $\mathbf{q}^m_{3,[\tau]}$. For each $\tilde{\mathbf{u}}^{\mathbf{q}_3^m}_{[\tau]} \in \mathrm{aff}^4_{[\tau]}(\mathbf{q}_3^m)$, there exist $\tilde{\mathbf{u}}^{\mathbf{q}_1^{m-1}}_{[\tau]} \in \mathrm{aff}^4_{[\tau]}(\mathbf{q}_1^{m-1})$ and $\tilde{\mathbf{u}}^{\mathbf{q}_2^{m-1}}_{[\tau]} \in \mathrm{aff}^4_{[\tau]}(\mathbf{q}_2^{m-1})$ so that

$$\begin{aligned}
\tilde{\mathbf{u}}^{\mathbf{q}_3^m}_{[\tau]} &= \frac{1}{2}\tilde{\mathbf{u}}^{\mathbf{q}_1^m}_{[\tau]} + \frac{1}{2}\tilde{\mathbf{u}}^{\mathbf{q}_2^m}_{[\tau]} \\
&\underset{(39)}{\overset{(35)}{=}} \frac{1}{2}\left(\mathbf{p}_0 + \lambda^{m-1}(\mathbf{p}_1 c_\tau + \mathbf{p}_2 s_\tau)\right. \\
&\qquad \left. + \frac{2\mu^{m-1}}{3}(\mathbf{p}_3 + \mathbf{p}_4 c_{2\tau} + \mathbf{p}_5 s_{2\tau}) + \mathrm{O}\left(\frac{1}{8^{m-1}}\right)\right) \\
&\quad + \frac{1}{2}\left(\mathbf{p}_0 + 2\lambda^{m-1}(\mathbf{p}_1 c_\tau + \mathbf{p}_2 s_\tau)\right. \\
&\qquad \left. + \frac{11\mu^{m-1}}{3}(\mathbf{p}_3 + \mathbf{p}_4 c_{2\tau} + \mathbf{p}_5 s_{2\tau}) + \mathrm{O}\left(\frac{1}{8^{m-1}}\right)\right) \\
&= \mathbf{p}_0 + 3\lambda^m(\mathbf{p}_1 c_\tau + \mathbf{p}_2 s_\tau) \\
&\quad + \frac{26\mu^m}{3}(\mathbf{p}_3 + \mathbf{p}_4 c_{2\tau} + \mathbf{p}_5 s_{2\tau}) + \mathrm{O}\left(\frac{1}{8^m}\right), \quad \boxed{\checkmark}
\end{aligned} \tag{40}$$

proving (30) for $i = 3$. The final two cases $i \in \{4,5\}$ are shown similarly.